Tutor/s

Dr. Xavier Giménez Font
Departament de Ciència dels Materials i Química Física

Dr. Daniel Bahamón García
Departament de Enginyeria Química i Química Analítica

Grau en Enginyeria Química

Treball Final de Grau

Molecular Modelling of Industrial Gases Separation by Adsorption on Metal-Organic Frameworks

Marta Tur Marí

June/2018

UNIVERSITAT DE BARCELONA

I was taught that the way of progress was neither swift nor easy
Marie Curie

En primer lugar, agradecer al Dr. Xavier Giménez y el Dr. Daniel Bahamón por permitirme formar parte de este proyecto, principalmente por la ayuda brindada durante el proceso. Gracias por entender mi situación desde el primer momento y adaptarse a ella. A todos los profesores que han formado parte de mi educación: desde los que me iniciaron en los números hasta los que me han enseñado el verdadero significado de estos.

A mis padres, por confiar siempre en mí y dejarme volar aun echándome de menos. *Gràcies papà per ser s'home més fort del món i superar-ho tot amb un somriure; gràcies mamà per cuidar-mos sempre, massa.* Gracias también a mi hermana, por estar día a día a mi lado sin importar la distancia que nos separa y sobre todo por regalarnos la alegría de la casa: a Anna. *Que tot lo bo sigui sempre per tu, rateta.*
A mis compañeros de piso: Alba, Luís y Rocío, por aguantarme en este periodo y crear un hogar a cientos de kilómetros de casa. A Cata, por ser un imprescindible en esta etapa y a todos los compañeros con los que he compartido horas de clases, laboratorios, biblioteca, bar… y se han acabado convirtiendo en amigos. Todos vosotros habéis hecho que este ciclo haya sido mucho mejor, gracias.

CONTENTS

SUMMARY

With the continuous growth of global energy demands and consequent climate change, the mitigation/elimination of the CO_2 released from combustion has become a main goal. Therefore, new materials applied in the capture of this component have gained great interest in recent years. Metal Organic Frameworks (MOFs) are an example of this.

In this project, in particular, the adsorption capacity of a specific MOF called Ni-MOF-74 is studied, since good results have been obtained a priori for pure CO_2 adsorption with this material. The carbon dioxide separation from different mixtures present in energy generation cycles is evaluated, including post-combustion gases, syngas and biogas. Computational simulation has been used to that end (specifically the Monte Carlo's method), which the aim to obtain adsorption isotherms for pure components and in mixture. The results obtained have been complemented with process simulations using typical mass and energy balances, identifying the most suitable regeneration technology for the separation of each one of the mixtures by using this material.

Keywords: CO_2 capture, adsorption, Metal Organic Framework, molecular simulations

RESUMEN

Con el continuo crecimiento de las demandas energéticas mundiales y consecuente cambio climático, la reducción/eliminación del CO_2 liberado por combustión se ha convertido en un objetivo principal de nuestra civilización. Por ello, nuevos materiales aplicados en la captura de este compuesto han ganado gran interés en los últimos años. Son un ejemplo de ello las estructuras órgano-metálicas (MOFs, por sus siglas en inglés, *Metal Organic Frameworks*).

En este trabajo, en concreto, se estudia la capacidad de adsorción de una estructura específica de MOF, conocida como Ni-MOF-74, que a priori ha dado buenos resultados con respecto a la adsorción de dióxido de carbono puro. Se ha evaluado la separación del dióxido de carbono en distintas mezclas usualmente presentes en los ciclos de generación de energía, incluyendo gases de post-combustión, gas de síntesis y biogás. Para ello se ha empleado la simulación computacional (específicamente el método Monte Carlo) con el objetivo de obtener isotermas de adsorción de componentes puros y en mezcla. Los resultados obtenidos se han complementado con simulaciones de proceso mediante balances típicos de materia y energía, identificando así el proceso de regeneración más apropiado para la separación con este material en cada una de las mezclas estudiadas.

Palabras clave: captura de CO_2, adsorción, Metal Organic Frameworks, simulación molecular

1. INTRODUCTION

The fast growth in global population and the industrialization of more and more countries has given rise to the upsurge in energy consumption which, by 85%, is being supported by the burning of fossil fuels [1]. This method releases large amounts of carbon dioxide into the atmosphere (80% of CO_2 emissions worldwide [2]) and is expected to continue increasing in the future due to the inherent energy density, abundance, and the economic dependence of modern society on these resources.

The ultimate goal of humanity should be to achieve a society supplied by clean energy requirements, nevertheless this changes requires modifications in the current energy framework. For this fact, Carbon Capture, Sequestration and Utilization (CCSU) technologies, that efficiently capture carbon dioxide from existing emission sources, can be a good alternative to reduce these emissions to the atmosphere. Furthermore, the Intergovernmental Panel on Climate Change (IPCC) has estimated that emissions could be reduced by 80-90% for a modern power plant equipped with appropriate CCSU technologies [3]. However, the development of these technologies could be more supported if the CO_2 demand increases exponentially by revaluing it.

With the purpose of capturing the CO_2, adsorption process based on porous solids have the potential to be more energy efficient than traditional adsorption process based on liquid solvents [4]. For this reason, several materials have been proposed for use as adsorbents such as Metal-Organic Frameworks (MOFs). MOFs are nanoporous crystalline materials formed by organic the self-assembly of metal ion vertices connected by organic linkers. Due to their large internal surface areas, high uptake of CO_2 and excellent tenability, MOFs have been regarded as a promising class of materials for CO_2 separation [5].

In specific, The M-MOF-74 family, also known as M-CPO-27 or M/DOBDC, has a large adsorption capacity and selectivity for CO_2 over many gases [6]. This MOFs are composed of first-row transitional metal nodes (M= Mg, Mn, Fe, Co, Ni, Cu or Zn) linked by 2,5-dioxido-1,4-benzenedicarboxylate linkers to form one-dimensional hexagonal channels lined with

coordinately unsaturated metal sites. Its open metal sites provide strong binding for guest molecules and bestow the frameworks with remarkable capacities and selectivities for CO_2 over more weakly binding gases like N_2, H_2 and CH_4. Although the best known and studied structure is Mg-MOF-74, in this project the behavior of Ni-MOF-74 will be studied. Although the first one presents higher adsorption, the latter one promises a greater desorption [2]. And since the efficacy for carbon capture depends dramatically on the regeneration process, Ni-MOF-74 could be promising for swing adsorption processes such as Vacuum Swing adsorption (VSA), Pressure Swing Adsorption (PSA) and Temperature Swing Adsorption (TSA). This study could be realized experimentally, although it is difficult to determine a mixture of gases. Therefore, simulation is an attractive tool in this analysis.

In order to obtain these results, computer simulations are extensively used. Computational methods have become an important and useful part of mathematical models of many science systems such as physicals, geophysics, astrophysics, chemistry and biology [6]. In the present study, specifically, Monte Carlo simulations are useful to reduce the time invested and to avoid the synthesis of molecules and the execution of experiments. The working of the Monte Carlo method is based on the use of random numbers and to get to describe the behavior of a system or explain a phenomenon difficult to understand and to treat analytically.

In consequence, the gas mixtures commonly used in electrical energy production, formed by this components, will be studied in this project: post-combustion gases, syngas and biogas. Therefore, CO_2/N_2, CO_2/H_2 and CO_2/CH_4 separations have been carried out with a total of 121 simulations which has led to 15000 hours of CPU (Central Processing Unit).

In conclusion, the obtained results inform that Ni-MOF-74 is a suitable material for CO_2 adsorption in post-combustion gases by using VSA methods, improving the energetic index consumption of the current technology: absorption with amines. It should be noted that this method is effective in the absence of impurities (*e.g.*, SO_2), since the energetic requirements can be increased with very small amounts. In addition, it has been specified that for a syngas mixture, carbon dioxide can be separated before or after combustion with no further energy demand changes, while the most appropriate sequence in biogas mixtures is to carry out a combustion in the presence of CO_2 and then perform the CO_2/N_2 separation.

2. OBJECTIVES

The main objective of this project is to evaluate whether Ni-MOF-74 could be a suitable material for CO_2 capture. Therefore, the adsorption of carbon dioxide with this material in mixtures of gases present in electrical energy production will be studied including post-combustion, syngas and biogas. More concrete goals are the following:

- Validate the simulation results obtained versus the experimental ones.
- Check the CO_2 adsorption capacity with respect to the remaining components present in the studied mixtures.
- Calculate the most suitable swing adsorption process for CO_2 capture from post-combustion gases, (with and without including SO_2 as impurity), and compare their energy consumption with that required in current technologies.
- Repeat the previous process for synthesis-gas and biogas, in addition to studying the best sequences of separation for these mixtures.

3. FUNDAMENTALS OF ADSORPTION

3.1. CO2 CAPTURE TECHNOLOGIES

Separation processes require exploiting the differences in molecular and thermodynamic properties of the components in the mixture. Currently, there are several useful technologies to separate carbon dioxide from mixed streams based on these differences. The most used methods will be explained below [7].

- Absorption is the most extended in the chemical and petroleum industries nowadays. Absorption falls into two categories: (1) physical, which is temperature and pressure dependent and (2) chemical, which is acid-base neutralization dependent.

The most common method is the *amine-based chemical adsorption* based on the exothermic reaction of a sorbent with the carbon dioxide present in the gas stream usually at room temperature [8]. The industrially preferred solvent is the monoethanolamine (MEA), followed by ammonia solutions, Selexol, Rectisol, and fluorinated solvents. Despite achieving carbon dioxide with high purity, liquid amines suffer degradation during regeneration and present a significant parasitic load on a power plant, on the order of one third of the energy generated [8].

- Cryogenic distillation has been used in liquid separations for a long time. It uses a principle of separation based on cooling and condensation but it also requires a huge energy demand. Nevertheless, this method can be adopted in oxygen production for oxyfuel combustion when the gas stream contains high CO_2 concentration. [7]

- Membrane-based separation is a growing technology; since the first implementation for gas separation membranes, it has been widely used in many industrial separation processes.[9] Membranes separate specific components from a mixture of gases in a feed stream by means of different mechanisms: (1) solution/diffusion, (2) adsorption/diffusion, (3) molecular sieve and ionic transport [8]. Although a high CO_2 separation efficiency can be obtained, it has disadvantages

such as lack of stability under the reforming environment and it is still in the research development phase.

- Biological methods have recently gained great interest in the capture of CO_2 with techniques like *algae bio-fixation of* CO_2 and the research using chemoautotrophic microorganisms which use inorganic chemicals instead of light energy for CO_2 removal. [8]

As mentioned in the previous points, there are several challenges and shortcomings in terms of the existing carbon capture technologies. Despite having technologies that can achieve a high amount of CO_2 captured, they increase the energy consumption by at least 25-35% [8]. Adsorption with porous materials is an alternative capture technology that can improve the energy efficiency using swing adsorption cycles (pressure, vacuum or temperature) for regeneration, with similar CO_2 recovery rates. These are the reasons why this has been the method selected to be studied, so it will be commented deeply in the next section.

3.2. ADSORPTION

Adsorption is a separation process whereby an increase in the concentration of a dissolved substance at the interface of a condensed and a liquid phase due to the operation of surface forces [10]. The adsorption process arises due to the presence of unbalanced or residual forces at the surface of the solid phase. These unbalanced residual forces have tendency to attract and retain the molecular species which comes in contact with the surface (it is essentially a surface phenomenon). This process involves two components: *adsorbent* and *adsorbate*; adsorbent is the material in which adsorption takes place, and adsorbate the substance which is being adsorbed on the surface of adsorbent. *"Adsorbate gets adsorbed".*

All adsorption processes involve two main steps: adsorption and desorption. During adsorption step, adsorbed gas molecules accumulate on the solid adsorbent surface. Desorption is the phenomenon of removing substances from the surface and thus regenerating the adsorbent for use in the next adsorption cycle [11]. The amount adsorbed is related to the dynamic equilibrium between adsorbent and adsorbate, and that normally mainly depends on the temperature conditions: the higher the adsorption rate (and lower desorption rate), the greater available fraction of the surface that will be covered by the material adsorbed at the equilibrium.

Adsorption forces, acting between adsorbate and adsorbent, can be classified into two main groups: (1) *van der Waals forces,* directly correlated with adsorbate molecular polarizability and (2) *electrostatic forces* such as surfaced field-molecular dipole interactions and surface field gradient-molecular quadrupole interactions. Adsorption is usually promoted by synergies between these different types of interactions [12].

Moreover, depending on the strength and nature of the bond between adsorbate and adsorbent, two types of adsorption can be distinguished: **physical adsorption** and **chemical adsorption**, which will be explained below.

- **Physical adsorption**, also called physisorption, is a process in which electronic structure of the atom or molecule is barely perturbed upon adsorption. Physisorption is due to weak attractive forces (generally van der Waals forces) which are originated from the interactions between electric forces.

- **Chemical adsorption**, also called chemisorption, is a kind of adsorption which involves a chemical reaction between the surface and the adsorbate, generating new chemical bonds at the adsorbent surface. These bonds are stronger which makes the binding energy higher (over 80 kJ/mol) and the desorption more difficult.

3.2.1. ADSORPTION ISOTHERMS

Porous materials can be defined in terms of their adsorption properties. Adsorption of a gas can be described quantitatively by an adsorption isotherm, *i.e.*, the amount of gas adsorbed by the material -at a fixed temperature- as a function of pressure. Porous materials are most frequently characterized in terms of pore sizes derived from adsorption data, and IUPAC conventions have been proposed for classifying them.

Depending on the predominant pore size, the porous solid materials are classified by IUPAC as: (1) **microporous materials**, having pore diameters up to 2.0 nm; (2) **mesoporous materials** having pore sizes intermediate between 2.0 and 50.0 nm; and (3) **macroporous materials**, having pore sizes exceeding 50.0 nm.

The IUPAC classification of adsorption isotherms is illustrated in Figure 1 [13].

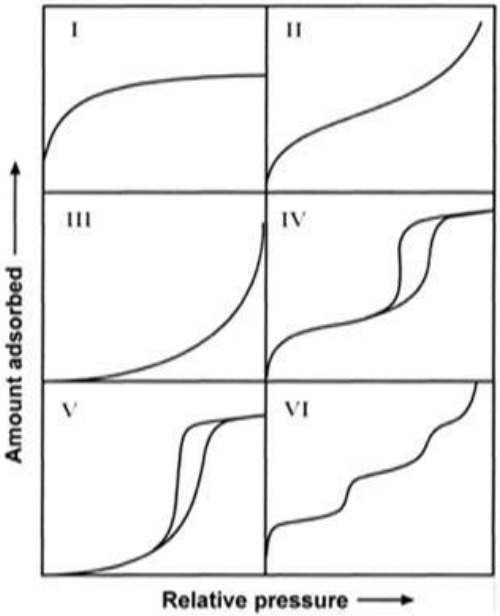

Figure 1. IUPAC classification of adsorption isotherm types.

The different types will be explained below.

- Type I isotherms are given by microporous solids having relatively small external surfaces. This isotherm is concave and the amount adsorbed approaches a limit value. This limiting uptake is governed by the accessible micropore volume rather than by the internal surface area. Sometimes it is called Langmuir isotherm.

- Type II isotherms are given by most gases on nonporous or macroporous adsorbents. The shape is the result of unrestricted monolayer-multilayer adsorption. The first inflection usually corresponds to the completion of the monolayer coverage. A more gradual curvature as pressure increases is an indication of overlapping and the onset of multilayer adsorption.

- Type III isotherms are given on nonporous or macroporous adsorbents, but in this case, there is no inflection point and therefore no identifiable monolayer formation; the adsorbent-adsorbate interactions are relatively weak and the adsorbed molecules are clustered around the most favourable sites. In contrast to Type II isotherm, the amount adsorbed remains finite at the saturation pressure.

- Type IV isotherms are given by mesoporous adsorbents. The adsorption behaviour is determined by the adsorbent-adsorbate interactions and also by the interactions between the molecules in the condensed state. A typical feature of Type IV isotherms is a final saturation plateau of variable length. The capillary condensation can be accompanied by hysteresis when the pore exceeds a certain critical width.

- Type V isotherms are given by materials where the adsorbent-adsorbate interactions are relatively weak. For instance, Type V isotherms are observed for water adsorption on hydrophobic microporous and mesoporous adsorbents.

- Type VI isotherm is representative of layer-by-layer adsorption on a highly uniform layer, while the sharpness of the step is dependent on the system and the temperature.

3.3. USEFUL ADSORPTION PARAMETERS

The essential requirement for an adsorption process is finding an adsorbent that preferentially adsorbs one component from a mixed feed. Furthermore, the adsorbent materials must satisfy some important criteria to be both economical and operational. The criteria for selecting the best adsorbent will be listed in this section.

3.3.1. ADSORPTION CAPACITY

The adsorption capacity of an adsorbent material is represented by its equilibrium adsorption isotherm. This parameter has a great importance for the capital cost of the adsorption equipment, since it determinates the amount of adsorbent required for a fixed volume bed.

In practice, it is preferred to use the **working capacity**, since it takes into account the amount of adsorbent that can be truly recovered for further uses.

3.3.2. WORKING CAPACITY (REGENERABILITY)

The working capacity (Δq) is the difference between the amount adsorbed at adsorption condition, and the amount desorbed in the desorption step. This capacity is strongly influenced by temperature and pressure. Furthermore, it is affected by the strength of the gas-solid interactions and the number of adsorption sites available.

$$\Delta q = q_{ads} - q_{des} \quad (1)$$

As mentioned, this parameter reports the amount of adsorbent that can be truly recovered during the adsorption/desorption cycles. Thus, the ease of regeneration will reduce the costs of the adsorption process.

3.3.3. HEAT OF ADSORPTION

The heat of adsorption is a measure of the strength of interactions between adsorbate and adsorbent. It is often referred to as **isosteric heat of adsorption,** q_{st}, and can be obtained from the Clausius-Clapeyron equation. From process engineering point of view, the adsorption heat is a measure of the energy required for the regeneration of the adsorbent and provides an indicator of temperature's variations that can be expected in the bed during adsorption (and desorption) under adiabatic conditions.

3.3.4. SELECTIVITY

The selectivity is based on the difference in affinities of the adsorbent for the different species constituting the fluid phase, and has a direct impact on the purity of the captured component (CO_2).

Given an adsorbent and a binary gas mixture in which A is the most strongly adsorbed component and B the predominant (but least strongly adsorbed), the equilibrium selectivity is generally expressed by using the separation factor:

$$\propto_{A.B} = \left(\frac{x_A}{x_B}\right) \cdot \left(\frac{y_B}{y_A}\right) \simeq \frac{K_A}{K_B} \quad (2)$$

where x and y are the molar fraction of species at the adsorbed and fluid phase, respectively. It can be shown that in many cases, $\propto_{A.B}$ can be calculated as the ratio between A and B Henry's constants (K_A, K_B) [14].

To select the appropriate adsorbent, in addition to the parameters previously mentioned, it must be also taken into account the *adsorption/ desorption kinetics*, the *mechanical strength of the sorbent particles,* the *chemical stability, the tolerance to impurities* and the *sorbent costs.*

3.4. ADSORBENTS

As it has been commented in the previous section, choosing the most suitable adsorbent is an important task. For the specific case of this study, the adsorbent must have affinity for CO_2 capture from a gas stream in which its other components can be N_2, CH_4 or H_2, and that, in addition, may contain impurities.

Over time, a large number of adsorbent materials have been considered for this CO_2 capture such as activated carbon, zeolites and zeolites-like materials, and Metal Organic Frameworks (MOFs).

3.4.1. ACTIVATED CARBON

Activated carbons (ACs) are the most investigated and widely used as adsorbent in industrial applications. ACs are made out of carbon-containing biological materials such as coals, industrial by-products and wood or other biomass materials (see Figure 2), providing them with the advantage of low cost and a suitable thermal stability. In addition, there is a broad variety including different pore size distributions and active surface areas.

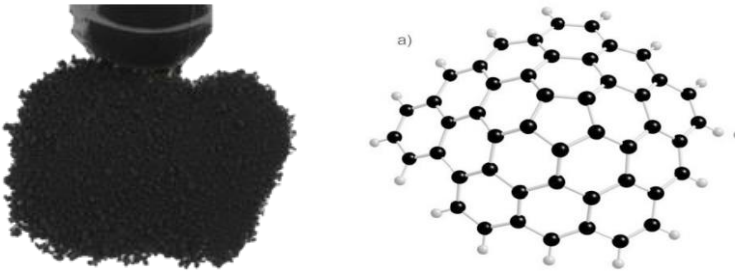

Figure 2. Typical activated carbon structure.

However, ACs have some restrictions such as limited CO_2 capture at high pressure or low temperature, low adsorption capacity and selectivity at low partial pressures of CO_2, and a harmful effect on the presence of contaminants.

3.4.2. ZEOLITES

As seen in Figure 3, zeolites are crystalline microporous aluminosilicates with large internal specific surface areas and volumes that can be found naturally or be synthesized. Its structure consists of periodical array of TO_4 tetrahedra (T=Si or Al) in which the Si/Al ration can be varied to control the adsorption properties [8]: zeolites with low Si/Al ratio are ones of the promising adsorbents for CO_2 adsorption and separation applications.

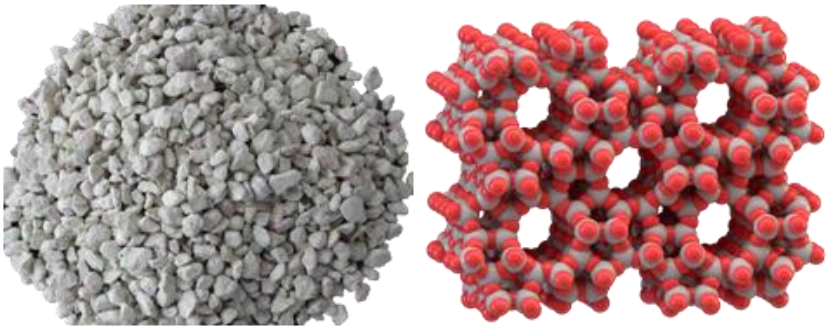

Figure 3. Zeolites structure.

Nevertheless, CO_2 adsorption on zeolites is strongly affected by temperature. Moreover, zeolites are strongly sensitive to water content because their highly hydrophilic character prioritizes the water adsorption instead of CO_2. In these cases, a very highly regeneration temperature is required (often in excess of 300ºC) which suppose an extra cost in the process [8].

3.4.3. METAL ORGANIC FRAMEWORKS

Metal Organic Frameworks (MOFs) are a new class of crystalline porous materials that are comprised of three-dimensional organic-inorganic hybrid network formed by metal-based nodes linked principally by organic ligand bridges and assembled though strong coordination bonds. Figure 4 shows a typical MOF framework at micro and nanoscale, and Figure 5 shows the most typical families studied in literature.

These materials have attracted much recent attention owing to their enormous structural and chemical diversity including: robustness, high surface area (up to 5000 m^2/g), high thermal and chemical stabilities, high void volume (55-90%), low densities (0,21-1 g/cm^3), and hence, with potential applications in gas storage, ion exchange, molecular separation, drug delivery, and heterogeneous catalysis [8].

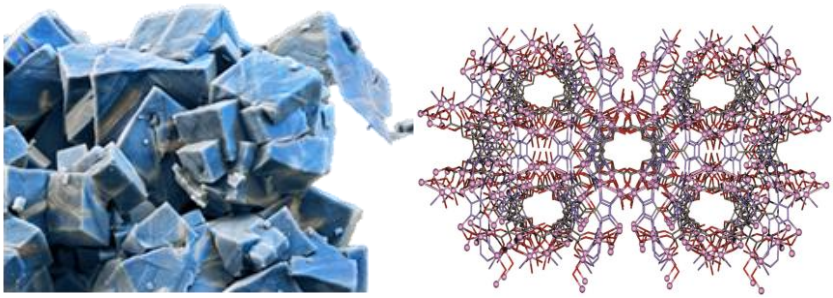

Figure 4. Typical MOF structure.

MOFs can be tuned and designed systematically by employing a so-called modular synthesis, wherein metal ions and organic ligand are combined to afford a crystalline, porous network. This

remarkable and easy tunability characteristic allows facile optimization of the pore structure, surface functions, and other properties for specific applications as porous materials, which differentiate these materials from other adsorbents.

They also present a reduced heat capacity over other capture technologies, and CO_2 adsorption processes in some MOF materials are fully reversible. Due to these facts, these materials are worthy candidates for the capture of CO_2 since they present a promising regeneration. For instance, the U.S. Department of Energy (DOE) issued a carbon sequestration program in 2009 aiming to achieve 90% CO_2 capture at an increase in the cost of electricity of no more than 35% by 2020, and one of the technologies proposed is adsorption with MOFs [8].

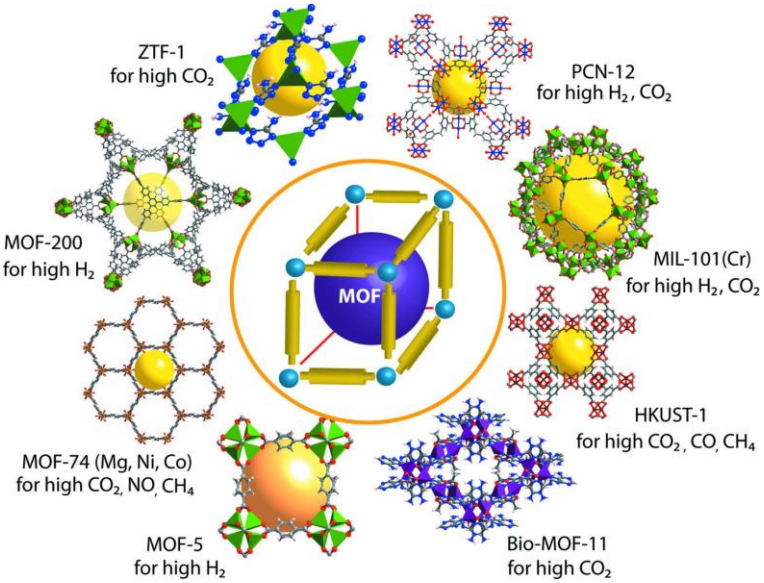

Figure 5. Most studied MOF types in literature [14].

3.4.3.1. Ni-MOF-74

M-MOF-74 family, also known as M-CPO-27 or M/DOBDC, are basically metal binding sites formed after the removal of axial ligands of metal atoms by thermal activation or other methods. This material structure is formed by carbon (grey in the Figure 6), oxygen (red in the Figure 6) and a metal (which can be Mg, Ni, Co or Zn, and is represented in blue in the Figure 6). They can offer extra binding sites to the guest molecules, especially at low pressures [15]. Besides,

this type of MOF presents the unique advantage, over other MOFs, of having unsaturated coordinated metal sites that can be varied without affecting the underlying structural framework [16].

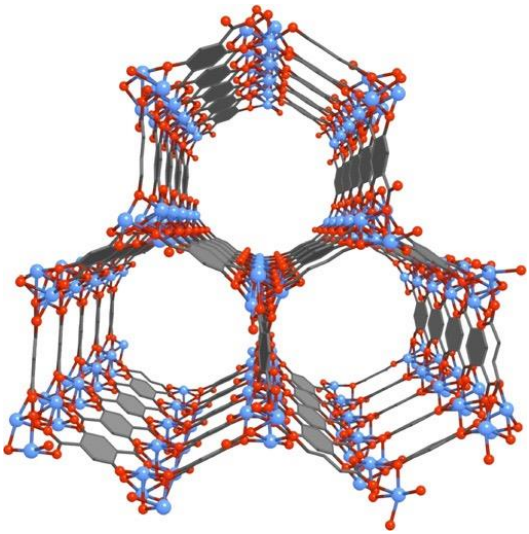

Figure 6. M-MOF-74 structure [17].

This study is focused on adsorption in specific of the structure with nickel metal centres. Ni/DOBDC was first synthesized as typical MOF by Pascal et al. [17] It consists of hexagonal packing of helical O_5Ni chains connected by 2,5-dihydroxyterephthalte linkers. In Figure 7, the structure of the material can be observed in more detail, where carbon is represented in grey, oxygen in red, hydrogen is white and the nickel in blue.

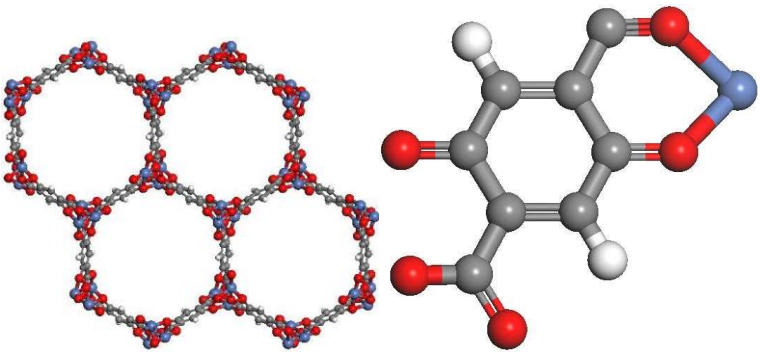

Figure 7. Ni-MOF-74 molecular structure [17]

This microporous material present pore volumes of around 7-8 nm, has high stability, large CO_2 capacity and long-term storage capability, as previously reported in literature. [18]

However, Ni-MOF-74 is considered to have hydrophilic surfaces which have strong interactions with H_2O molecules. Kizzie et al. [19] observed that Ni-MOF-74 retains approximately 60% of its initial capacity under dry condition.

Therefore, since CO_2 adsorption capacities decrease when H_2O molecules are presents, it is advantageous to utilize a guard bed to adsorb water thereby minimize H_2O effects on the adsorbent targeted for CO_2 capture. For this reason, clear streams of water will be studied in this project, assuming a water filter prior to adsorption.

3.5. SWING ADSORPTION PROCESSES

Adsorption-based separation processes require both adsorption and desorption stages. The adsorbent regeneration (or desorption) can be achieved by using **swing adsorption processes** which make use of the differences between the tendencies for adsorption of the individual components in a gas mixture.

The most common swing adsorption methods use a cycling variation of the pressure or temperature: **Pressure Swing Adsorption (PSA), Vacuum Swing Adsorption (VSA)** and **Temperature Swing Adsorption (TSA)**.

In order to maintain a continuous stream product, they are operated with multiple beds containing a stationary adsorbent and use a manifold of valves to switch gas flow to the beds corresponding to adsorption and desorption cycles, as can be seen in Figure 8.

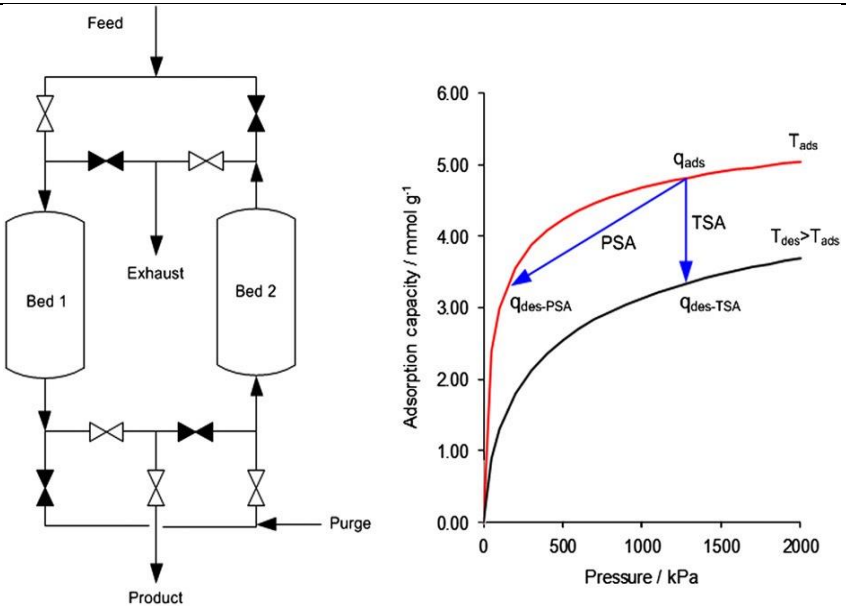

Figure 8. Schematic representation of a swing adsorption System operation [20].

3.5.1. PRESSURE SWING ADSORPTION

In the PSA method, adsorption occurs at elevated pressure and the desorption at near-ambient pressure. The PSA processes typically purify weakly adsorbing species from gaseous mixtures with strongly adsorbing species.

Chaffe et al. [21] has indicated that this process is too expensive for CO_2 capture, so it is likely that conventional PSA process will be difficult to implement in a large flow of gas due to the technical difficulties in the pressurization step.

3.5.2. VACUUM SWING ADSORPTION

The VSA method is similar to the PSA method, altering the adsorption/desorption pressure conditions. In this case, the adsorption step occurs at atmospheric pressure and the component is recovered at sub-atmospheric pressures.

3.5.3. TEMPERATURE SWING ADSORPTION

In the TSA, the adsorbent is regenerated by desorption at a higher temperature than used during the adsorption. The temperature of the bed can be increased by purging the bed with hot, inert and non-adsorbing gas, or by heat transfer from heating coils located within the bed. After desorption, the bed temperature is reduced and the adsorption cycle starts again.

In addition to these methods, it is very common to find a combination of them. Choosing the correct method of regeneration is a key factor to reducing the energy requirement.

In the present text VSA, PSA, TSA methods and the combination of vacuum and pressure swing adsorption (VPSA) will be compared.

3.6. CO_2 STREAMS FROM INDUSTRIAL PROCESSES

3.6.1. POST-COMBUSTION

The post combustion gas is the result of the exothermic reaction of a hydrocarbon in the presence of air in order to obtain energy. If the hydrocarbon is methane, there are a series of steps involved in combustion: it is believed that methane first reacts with oxygen to form formaldehyde which is broken down into formyl radical and gives carbon dioxide and water, according to the following reaction:

$$CH_4 + 2O_2 \rightarrow CO_2 + 2\,H_2O$$

If the oxygen used comes from air and taking into account a complete reaction without excess air, the result is a gas stream of carbon dioxide, water and nitrogen. Removing water, a mixture of about 85% N_2 and 15% CO_2 is achieved.

With the aim of capturing CO_2, a process of CO_2/N_2 separation after combustion is necessary, since nitrogen is an inert gas that can be release into the atmosphere and CO_2 must be captured and stored.

3.6.2. SYNGAS

Synthesis gas, also known as syngas, is produced by gasification of a carbon containing fuel to a gaseous product with some heating value. It is often produced by gasification of coal or municipal waste in which carbon is combined with water or oxygen to give rise to carbon dioxide, carbon monoxide and hydrogen.

This mixture can be used as a fuel source although its energy density is 50% of that of natural gas [22]. To carry out this project, the following reactions for the synthesis gas production will be taken into account:

$$CH_4 + H_2O \longrightarrow CO + 3\,H_2$$

$$CO + 3\,H_2 + H_2O \longrightarrow CO_2 + 4H_2$$

It should be noted that to facilitate the simulations and in order to study the CO_2 separation, these reactions will be assumed as irreversible and complete, resulting in a stream of about 70-80% H_2 and 20-30% CO_2.

One of the uses of this syngas is as a fuel in an integrated gasification combine cycle (IGCC) power generation configuration. There are commercially available technologies to process syngas to generate industrial gases, fertilizers, chemicals, fuels and other products.

The CO_2 capture in this mixture can be done before or after combustion. The mixture of carbon dioxide and hydrogen can be used for combustion and subsequently separated, or can be separated previously and only use hydrogen as fuel.

3.6.3. BIOGAS

Biogas is a gas formed mainly by methane and carbon dioxide in different concentrations depending on the organic matter from which it has been formed. The main sources of biogas are

livestock and agro industrial waste, sludge from urban wastewater treatment plants (WWTPs) and the organic fraction of household waste.

The production of biogas occurs in anaerobic digesters through biological decomposition processes in the absence of oxygen. In these equipments, organic matter (substrate) is feed at certain operating conditions. In order to maximize the production of biogas in digesters, it is usual to mix different types of substrates. [23]

Biogas is the only renewable energy that can be used for any of large energy applications: electric, thermal or as fuel. Direct use can be applied in adapted boilers for its combustion, as well as, perform a CO_2/CH_4 separation prior to combustion. If biogas (50% CO_2 / 50% CH_4) is used directly as fuel, the next reaction will occur:

$$CH_4 + 2\ O_2 + CO_2 \rightarrow 2\ CO_2 + 2\ H_2O$$

If this technique is used, a CO_2/N_2 separation should be performed after combustion (with water separation first). A CO_2 capture prior to combustion can also be done, which will also lead a subsequent separation of CO_2/N_2.

3.7. CO_2 APPLICATIONS/USES

The current main issue about this component is the large amount produced and the low value of this. It is widespread that CO_2 is the main problem of the greenhouse effect, whose concentration in air has also been steadily increasing from year to year. Therefore, an important task nowadays is the revaluation of CO_2 as the demand of large amounts of this compound would accelerate the deployment of CCSU.

At the present time, CO_2 has several applications in the oil industry. In the Enhanced Oil Recovery process (EOR), it acts as a solvent that reduces the oil viscosity. It is also used as a fluid for the stimulation and fracturing of oil and gas wells. [24]

This compound is also widely used in the food industry including cooling while grinding powders such as spices, and inert atmosphere to prevent spoilage. CO_2 is commonly used in MAP (modified atmosphere packaging) and CAP (Controlled atmosphere packaging) because of its ability to inhibit growth of bacteria. It is also used in carbonating beverages, preventing wine oxidation during the maturation, and as a solvent for decaffeinating coffee. In addition, it is

used as an inerter in the pharmaceutical industry, as well as, for chemical synthesis, supercritical fluid extraction and transport of products at low temperature.

Another common use of this compound is that of fire suppression technology: in fire extinguishers and industrial fire protection systems. CO_2 provides a heavy blanket of gas that reduces the oxygen level to a point where combustion cannot occur.

As industrial applications it is worth mentioning its performance as a refrigerant gas. Other uses of CO_2 are: the reduction of pH during pulp washing operations, the re-mineralisation of water, in steel and metal manufacture, and in pneumatics. [25]

CO_2 can also be applied as a substitute to Portland cement in the formation of sodium bi-carbonate used to treat bauxite residues. Moreover, CO_2 can be permanently stored as an un-reactive limestone within concrete. Furthermore, it can be used as a liquid fuel forming: renewable methanol, formic acid and genetically engineered micro-organisms for direct fuel secretion. Its injection can also increase the yield of methanol from conventional methanol synthesis [25].

In addition to the aforementioned applications, there are some emerging uses that could re-value this compound exponentially, such as Enhanced coal bed methane recovery (ECBM) and enhanced geothermal systems (EGS).[24]

4. COMPUTATIONAL SIMULATIONS

The principles of molecular simulation are based on a system which has been modelled by describing interactions between the atoms. The Molecular Dynamic technique (determinist method) and the Monte Carlo technique (a stochastic method), have been two very important tools in the last years to gain insights in several physic-chemistry processes on microporous materials [26].

These methods are complementary and often alternative to the experimental methods with the objective of solving theoretical models in their total complexity through numerical resolution using computers.

4.1. INTERACTION POTENTIALS

The use of the interatomic potential of a system is important in both Molecular Dynamics and Monte Carlo simulations, since the accuracy of the results in relation to real processes will depend on this. However, the required computer time (CPU) also depends on this parameter. Therefore, it is important to determine the degree of precision we want to give to the system.

Potential function is used to define interactions among atoms. The total energy of a system of N atoms interacting with each other can be described by an empirical potential [27].

$$U = \sum_i U_1(r_i) + \sum_i \sum_{j>i} U_2\left(\vec{r}_i, \vec{r}_j\right) + \sum_i \sum_{j>i} \sum_{k>j} U_3\left(\vec{r}_i, \vec{r}_j, \vec{r}_k\right) + \ldots \qquad (3)$$

Furthermore, the potential has two main contributions: van der Waals and electrostatic forces.

4.1.1. VAN DER WAALS FORCES

Van der Waals forces are interactions distance-dependent between atoms or molecules that quickly vanish at longer distances. As they are not the result of any chemical-electronic bond,

they are weaker and more susceptible to being perturbed. These forces can present attractive forces between adsorbate and adsorbent because of the instant fluctuations of electric dipoles moments, and repulsive forces created by penetration or overlap of the electronic cloud between molecules and adjacent surfaces. Both forces are combined in the Lennard-Jones equation.

Lennard-Jones potential is used in simulations when the objective is to model general class of effects and the only requirement is to have a physically reasonable potential. The most used widespread model is the 12-6 Lennard-Jones given by the following equation.

$$U(r_{ij}) = 4 \cdot \varepsilon \left[\left(\frac{\sigma}{r_{ij}} \right)^{12} - \left(\frac{\sigma}{r_{ij}} \right)^{6} \right] \tag{4}$$

Where ε is the well depth (see Figure 9) which is a measure of how strongly the two particles attract each other, and σ is the distance at which the intermolecular potential between the two particles is zero.

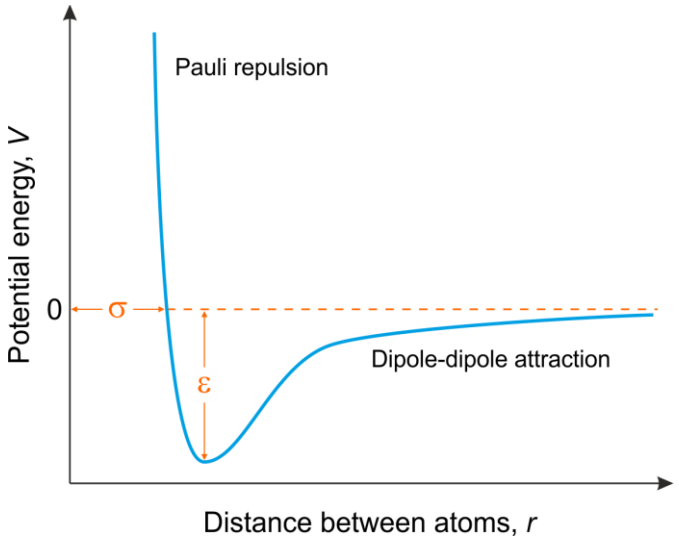

Figure 9. Lennard-Jones potential.

The term $1/r_{ij}^{12}$ denotes the repulsion between atoms when they are brought close to each other, and is related to the Pauli principle: when electronic clouds surrounding the atoms start to overlap, the energy of the system increases abruptly. The term $1/r_{ij}^{6}$, dominating at large distance, constitutes the attractive part and describes the cohesion to the system. This equation is usually

combined by Lorentz-Berhelot rules to describe interactions between different types of atoms/molecules.

$$\varepsilon_{ij} = \sqrt{\varepsilon_{ii} \cdot \varepsilon_{jj}} \; ; \; \sigma_{ij} = \frac{\sigma_{ii}+\sigma_{jj}}{2} \tag{5}$$

4.1.2. ELECTROSTATIC FORCES

Electrostatic phenomena arise from the forces that electric charges exert on each other. Such forces are described by Coulomb's law:

$$U_{elec}(r_{ij}) = \frac{1}{4 \cdot \pi \cdot \varepsilon_r \cdot \varepsilon_0} \cdot \frac{Q_i \cdot Q_j}{r_{ij}} \tag{6}$$

Where ε_0 is the vacuum permittivity ($8.85419 \cdot 10^{-12}$ $C^2 \cdot N^{-1} \cdot m^{-2}$) and Q_i and Q_j the charges of the atoms.

Since these forces are created by the electrical interactions between atoms, they are much stronger than the van der Waals interactions. In practice, we are often dealing with short-range interactions. In that case it is usually permissible to truncate all intermolecular interactions beyond a certain cut-off distance r_c.

4.2. BOUNDARY CONDITIONS

In a three-dimensional N-particle system with free boundaries, the fraction of all molecules that is at the surface is proportional to N'/3. In order to simulate bulk phases, it is essential to choose boundary conditions that mimic the presence of an infinite bulk surrounding our N-particle model system. This is usually achieved by employing periodic boundary conditions. The volume containing N particles is treated as the primitive cell of an infinite periodic lattice of identical cells, as shown in Figure 10.

A given particle (i, say) can now interacts with all other particles in this infinite periodic system, that is, all other particles in the same periodic cell and all particles (including its own periodic image) in all other cells.

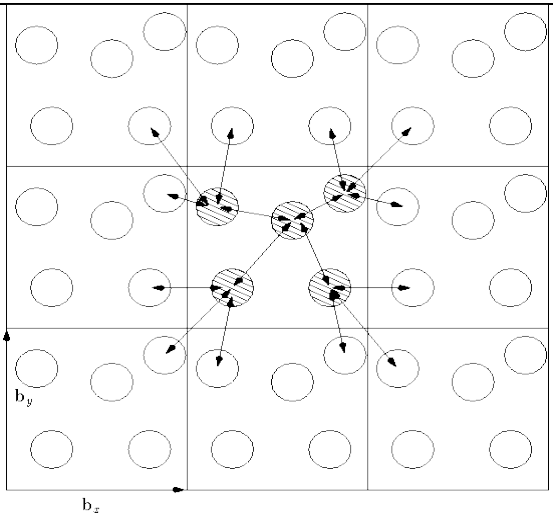

Figure 10. Schematic representation of periodic boundary conditions [28].

4.3. MONTE CARLO

Monte Carlo (MC) method is a statistical-stochastic technique based on the generation of different configurations of the phase space accessible to the system.

The advantage of this technique compared to MD simulations is that MC simulation does not have to follow the natural path of using Newton's laws of motion: a new configuration can be generated in such way that all diffusion barriers are avoided in the experimental configuration.

The configurations of a property M with the MC method can be calculated by the following expression [29].

$$\langle M \rangle = \frac{\int dP^N dr^N \, exp[-\beta H(p^N, r^N)] M(p^N, r^N)}{\int dP^N dr^N exp[-\beta H(p^N, r^N)]} \tag{7}$$

Where H is the Hamiltonian (*i.e.*, sum of all kinetic and potential energies) which depends on both momenta p and coordinates r. If the kinetic energy of the Hamiltonian is considered that depends on the square of the moment, these degrees of freedom can be dramatically integrated, and hence.

$$\langle M \rangle = \int dr^N M(r^N) Z(r^N) \tag{8}$$

Being Z(r^N) the system probability function:

$$Z(r^N) = \frac{exp[-\beta U(r^N)]}{\int dr^N exp[-\beta U(r^N)]} \tag{9}$$

These integrals are multidimensional, making this method impractical. An alternative solution is to generate points in the configuration space according to the distribution of Z probabilities.

$$\langle M \rangle = \frac{1}{N} \sum_{i=1}^{L} n_i M(r_i^N) \tag{10}$$

But this method is not optimum since the points with low energy contribute significantly while those with high energy will have little statically weight. Consequently, *Metropolis method* has been proposed which consist of generating points with importance sampling.

4.3.1. METROPOLIS METHOD

Metropolis method was introduced as Markov process [30] in which a random walk is constructed in such a way that the probability of visiting a point r^N is proportional to the Boltzmann factor exp[-$\beta U(r^N)$].

Therefore, it can be assumed that we have an atomic or molecular model system in a suitable starting configuration and that we have specified all intermolecular interactions. The next step is to set up the underlying Markov chain, *i.e*., we must decide how to generate trial moves. Trial moves that involve only the molecular centers of mass should be distinguished from those that change the orientation or the conformation.

For the translational moves, a perfectly acceptable method for creating a trial displacement is to add random numbers between -Δ/2 and +Δ/2 to the x, y and z coordinates of the molecular center of mass:

$$\begin{aligned} x'_i &= x + \Delta(Ranf - 0.5) \\ y'_i &= y_i + \Delta(Ranf - 0.5) \\ z'_i &= z_i + \Delta(Ranf - 0.5) \end{aligned} \tag{11}$$

Where *Ranf* are random numbers uniformly distributed between 0 and 1. And the equation to create a randomly rotation type is:

$$r' = \begin{pmatrix} cos(\Delta\theta) & -sin(\Delta\theta) & 0 \\ sin(\Delta\theta) & cos(\Delta\theta) & 0 \\ 0 & 0 & 1 \end{pmatrix} \tag{12}$$

Having these equations, the main way to construct such a random walk is the following scheme proposed [28].

1. Select a particle at random, and calculate its energy $U(r^N)$
2. Give the particle a random displacement, $r'=r+\Delta$, and calculate a new energy $U(r'^N)$
3. Accept the move from r^N to r'^N with probability:

$$acc(o \to n) = min(1, exp\{-\beta[U(n) - U(o)]\}) \qquad (13)$$

This shows that the probability of accepting or rejecting depends on the energy difference between the old (o) and new (n) conformation. In conclusion, this method is based on the minimization of the total energy of the system which is achieved in a large number of steps.

5. METHODOLOGY AND SIMULATION DETAILS

The adsorption and separation characteristics of Ni-MOF-74 were calculated using Monte Carlo simulation based on the Grand Canonical ensemble, in which the chemical potential (related to pressure), the temperature and the volume of the simulation box were constants (*also known as μVT ensemble*). The given temperature and pressure were input parameters, as well as the unit cell volume of the crystal (*i.e.,* adsorbent).

In the interest of carry out these simulations, it is necessary to describe the Force Field as accurately as possible, since it enables achieving the potential of each step of the simulation. To detail it, the LJ parameters are required for the molecules present in the system. It must be taken into account that Ni-MOF-74 has been treated as rigid molecule, with atoms fixed at their crystallographic positions during simulation. For describing the adsorption of pure components and mixtures, the Lennard-Jones parameters from Table 1 were used.

The atomic values for MOF were taken from Bekker et al. [31], TraPPE-UA parameters were used for CO_2, H_2, CH_4 and N_2 molecules [32], while the forcefield of Ketko *et al.* was used for SO_2 [33].

The results of each simulation have been achieved by performing one million Monte Carlo steps. The first 500,000 have been used as equilibration of the system, while an average of the following 500,000 production steps has been performed to obtain the number of molecules adsorbed at each T, P condition. An example of this can be observed in Appendix 1.

With the purpose of executing this project and better understand the CO_2 capture in different mixtures, a total of 121 simulations for both pure components and mixtures have been performed.

These MC results were used to calculate the adsorbed molecules and the isosteric heat, which can be computed with the following equation.

$$q_{st} = R\left(\frac{dlnp}{d(1/T)}\right) = R \cdot T - \frac{\langle \mathcal{N} \cdot U \rangle - \langle \mathcal{N} \rangle \cdot \langle U \rangle}{\langle \mathcal{N}^2 \rangle \cdot \langle \mathcal{N} \rangle^2} \quad (14)$$

MOLECULE	ATOM	σ (A)	ε (K)
MOF	Ni	2.52	7.45
	C	3.43	45.8
	O	3.12	27.93
	H	2.57	21.3
CO_2	C	2.8	27
	O	3.05	79
N_2	N	2.958	36.4
	COM (N_2)	--	--
H_2	O	3.02	27
	COM (H_2)	--	--
H_2O	H	3.1589	93.2
	COM (H_2O)	--	
CH_4	C	3.73	148
SO_2	S	3.620	145.9
	O	3.010	57.4

**COM: Center Of Mass*

Table 1. Lennard-Jones parameters used in MC simulations.

Where, $\mathcal{N}$ are the number of molecules adsorbed and U the total energy of the system, both given values of the simulation. R is the gas constant with a value of 8.314 [J/mol·K] and T the temperature at which the adsorption is carried out.

Moreover, in order to perform mass and energy balances of the adsorption bed, the properties from Table 2 were used.

In addition to the computational simulations, swing adsorption process has been studied for different gas mixtures such as post-combustion gas (with and without including impurities), syngas and biogas. To perform these comparisons, it is necessary to calculate the desorption works for each method.

Density	$\rho_{Ni\text{-}MOF\text{-}74}$ **[kg/m^3]**	1194
Heat capacity	$C_{p,Ni\text{-}MOF\text{-}74}$ **[kJ/kg·K]**	0.9
Bed voidage	ε	0.4
Bed volume	**V [m^3]**	1

Table 2. MOF bed parameters used.

- **Vacuum swing adsorption:** The energy required is the work necessary to apply vacuum in the bed, by decreasing the atmospheric pressure to a vacuum pressure. Therefore, the depressurization work is:

$$\boldsymbol{W = \left(\frac{k}{k-1}\right)\frac{R\cdot T}{\eta}\, q\left(\left(\frac{P_{des}}{P_{ads}}\right)^{\frac{k-1}{k}} - 1\right)} \qquad (15)$$

Where, k and η represent the politropic constant and the turbine efficiency respectively, and their values are described in Table 3. *R* is the gas constant with the value of 8.314 [J/mol·K] and *q* the amount adsorbed in [mol/kg]. P_{ad} is the pressure at which the adsorption occurs (1 atm) and P_{des} the pressure required for the desorption.

- **Pressure swing adsorption:** The work required is the necessary to pressurize the input current at a pressure higher than the atmospheric (3, 7 or 10 atm). Therefore, the same Eq. (15) can be used. However, in this case the pressure of desorption is 1 atm and the adsorption pressure is a higher one (3, 7 or 10 atm).

- **Temperature swing adsorption:** The energy required is the necessary to heat the bed from a temperature of 313 K to a higher one (*e.g.*, 413 K). Therefore, the heat required is:

$$\boldsymbol{Q = m \cdot (C_p \Delta T + \sum q_{st} \cdot \Delta q)} \qquad (16)$$

Where *m* is the mass of Ni-MOF-74 ($m = \rho.V.(1\text{-}\varepsilon)$) and ΔT the difference between the temperature of desorption and adsorption. Δq is the working capacity with the equation (1) and q_{st} the isosteric heat defined according to the equation (14).

In order to compare these different energy requirements, a scheme as the one shown in Appendix 2 has been used to calculate the total increase in energy due to coupling an adsorption system to a thermal plant. For the purpose to calculate these magnitudes, some additional parameters have been required (see Table 3).

POLYTROPIC CONSTANT	k	1.28/1.4
LHV METHANE	[KJ/kg]	47000
LHV HYDROGEN	[kJ/kg]	120000
HEAT CAPACITY OF GAS	Cp [kJ/kg·K]	1
TURBINE EFFICIENCY	η	0.75
THERMAL EFFICIENCY	η	0.85

** LHV: Lower Heat Value*

Table 3. Additional combustion parameters.

6. RESULTS AND DISCUSSION

6.1. VALIDATION

The first step in a molecular simulation study is to validate the results obtained to confirm the appropriateness of the force field used. In order to carry out this task, CO_2 isotherm was obtained using the Monte Carlo method at the temperature of 298K (which is the experimental data from Queen *et al* [34]. The CO_2 uptake, in moles per kilogram of MOF, have been represented for both cases where the crosses in orange are the experimental results and the green points the results obtained with Monte Carlo method (see Figure 11).

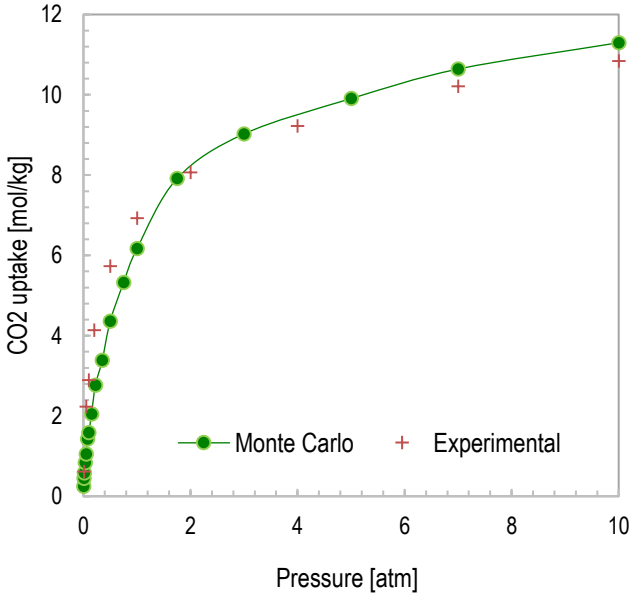

Figure 11. Pure CO_2 isotherm at 298 K. Validation vs experimental data from Queen et al. [34].

As it can be seen in Figure 11, the results obtained by simulation are close enough to the experimental ones, and therefore we can take this method as valid. Unfortunately, there are not numerous experimental studies including the full set of isotherm data using the selected MOF, being these the only experimental data available at conditions close the experimental ones (*i.e.,* 300-320K) for the studied molecules.

Another extra way that allows to obtain the molecular simulation is to determine the preferential sites of adsorption of the different molecules. As an example, in Figure 12 a snapshot of CO_2 adsorption at low pressures in Ni-MOF-74 is shown. In this figure, it can be observed that the dioxide carbon molecules have a great affinity for the unsaturated metal centres of the material (represented in blue). Firstly, the sites closest to the metal are filled and as the pressure increase (ie, more CO_2 molecules adsorbed), the carbon dioxide will be located where possible, filling the entire volume.

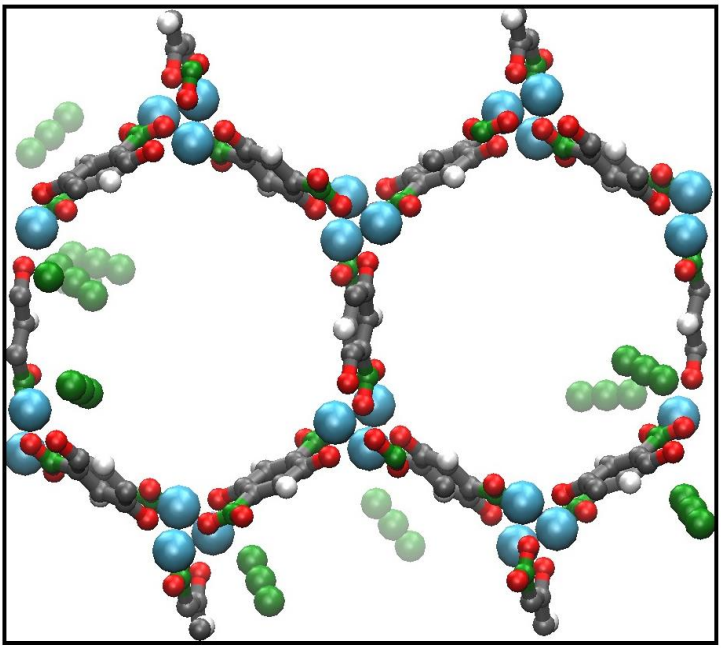

Figure 12. Snapshot of preferential adsorption sites of CO_2 in Ni-MOF-74 at 0.1atm.

6.2. ISOTERMS OF PURE COMPONENTS

Subsequently, the isotherms of pure CO_2 at different temperatures, as well as those of several components are shown in Figures 13 and 14.

6.2.1. PURE CO_2 ISOTHERMS AT DIFFERENT TEMPERATURES

In this subsection, CO_2 isotherms at different temperatures (298 K, 313 K, 413 K) have been calculated and compared. In this case, the error bars have been added in Figure 13 to show the dispersion of the MC results.

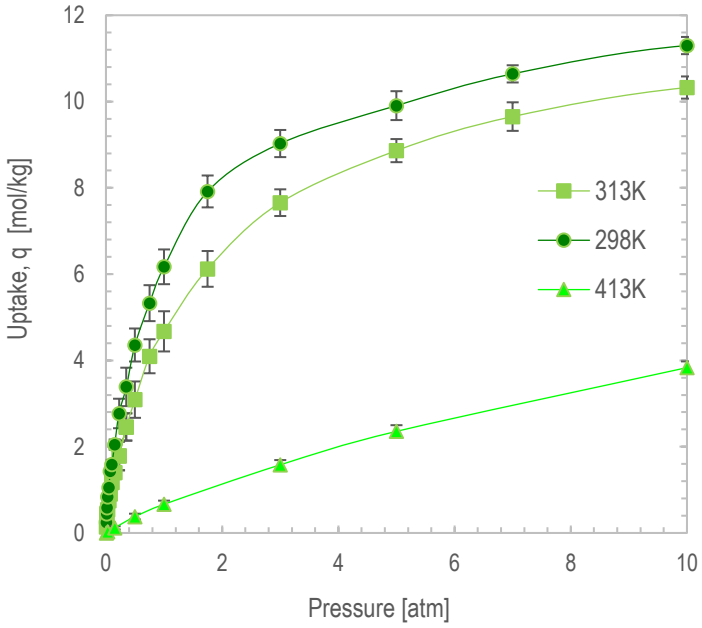

Figure 13. Pure CO_2 adsorption isotherms at diferent temperatures.

This figure is interesting for the purpose of calculating working capacities (Δq) in TSA cycles (See Figure 8 in section 3.1). It can be observed that the amount adsorbed decreases as the

temperature is increased. The difference between the adsorbed moles at one temperature and the ones adsorbed at a higher temperature will provide the bed with the possibility of regenerating by heating.

6.2.2. OTHER PURE COMPONENT ISOTHERMS

The adsorption isotherms of the pure compounds are important in order to know the effect that they will have in the system. When a process is going to be designed, it is essential to know the adsorption of the compounds of the mixture. These graphs cannot provide definitive conclusions on the mixture since it is necessary to take into account the compounds interaction, but it can give an idea of which components can have a better adsorption.

As mentioned, the compounds selected for this study were carbon dioxide (CO_2), nitrogen (N_2), sulphur dioxide (SO_2), hydrogen (H_2) and methane (CH_4). The reason why these components have been chosen is the fact that they are the main components of the mixtures which will be studied: post-combustion gases, syngas and biogas. It must be noted that as mentioned previously in section 4.1, the behaviour of water will not be studied in this project since it strongly reduces the CO_2 adsorption with only water traces. Its ease of elimination will lead to the assumption of a retreat prior to adsorption.

In Figure 14, adsorption isotherms of pure components have been plotted at the temperature of 313K and a pressure ranges from 0.005 to 10 atmospheres.

It can be seen that CO_2 has one the higher adsorption capacities in the selected MOF (with the exception of SO_2), which presents an adsorption ranges between 1-10 mol/kg. It is presumed to accomplish a suitable separation of CO_2 from the rest of the components in a mixture. Therefore, it can be deduced that Ni-MOF-74 can be a good candidate for the adsorption of CO_2 in the studied gas streams.

A remarkable fact is that the molecules with greater affinity with the MOF and therefore with higher adsorption, presents isotherms of type I and can be linearized by the Langmuir equation (*e.g.,* CO_2 and SO_2). However, it is noted that the adjustment for CO_2 could be improved with more complex isotherms proposed in literature. The components that show a lower affinity, practically present a linear function which adapts to the start of type III isotherms. These can be

linearized by Freundlich equation. The parameters of the Langmuir and Freundlich equations are presented in Appendix 2.

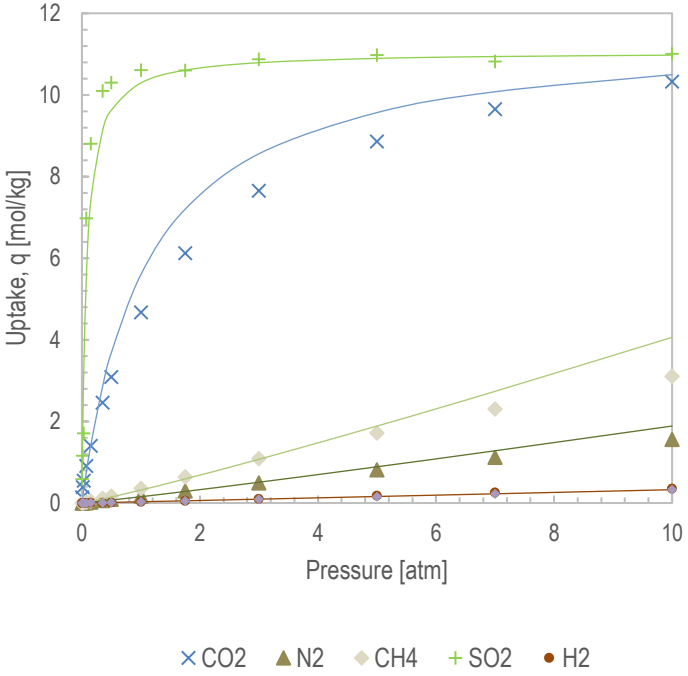

Figure 14. Adsorption isotherms of pure components at 313K. Symbols represent MC results and lines are linearization adjustments from Langmuir or Freundlich models.

It must be noted that SO_2 presents a high affinity for Ni-MOF-74 that rapidly reaches saturation of 11mol/kg at pressures below atmospheric. This fact could suppose a poisoning of the adsorbent since this element would occupy all the pores of the MOF. However, taking into account that sulphur dioxide is in a small amount in these flows (*e.g.,* between 0.2 and 1%), although the capacity of CO_2 adsorption will be decreased, it should not be an issue. (This is presented in detail in subsection 6.3.1.).

With the information extracted from the adsorption isotherms, the value of isosteric heats (q_{st}) can be deduced. This magnitude measures the energy necessary to remove a molecule that is in

its average vibrational state, under the force of attraction of the solid and its neighbours, and take it to a point located at an infinite distance from the solid. [20] Therefore, it will depend quantitatively on the adsorbent-adsorbate interactions: the greater affinity with Ni-MOF-74, the higher isosteric heat. Table 4 shows the isosteric heats obtained for each one of the aforementioned compounds.

MOLECULE	ISOSTERIC HEAT [KJ/MOL]
SO_2	45.2
CO_2	30.9
CH_4	13.6
N_2	12.6
H_2	5.7

Table 4. Isosteric heat for each molecule studied.

It can be observed that CO_2 and SO_2 have higher isosteric heats. This fact was to be expected. As mentioned above, this magnitude depends on the interactions between the compound and the MOF. Consequently, the compounds with superior affinity to MOF are those with higher isosteric heat as well as greater adsorption.

It should be noted that as the isosteric heat indicates how difficult is to remove a molecule from the adsorbent, the higher q_{st}, the more difficult the desorption will be, and it must be taken into account when calculating the energy requirements for material regeneration. In addition, values from Table 4 show that pure physisorption processes have been obtained, since all the q_{st} are not higher than 80 kJ/mol.

6.3. MIXTURES

Since it has been verified that Ni-MOF-74 material is a good possible adsorbent of CO_2, one of the most common gas streams have been studied, including post-combustion gases, syngas

and biogas. Therefore, simulations of binary CO_2/N_2, CO_2/H_2 and CO_2/CH_4 mixtures, as well as ternary $CO_2/N_2/SO_2$ separations with different SO_2 concentrations have been performed.

The following subsection is focused on the results obtained for the post-combustion mixture, as well as the effect of SO_2 as impurity in this stream. These gases have been the subject of study during the last years, since the technology currently used, as has been discussed in Chapter 3, are absorption with amine solvents. Then, it will be verified if the adsorption with Ni-MOF-74 can reduce the energy consumption, and therefore, be a better option than the current technology. In addition, the different methods of swing adsorption will be compared to know which is the most adequate for each mixture type.

6.3.1. CO_2/N_2 SEPARATION

First of all, CO_2/N_2 mixtures (15% CO_2; 85% N_2) were simulated at pressures of 1, 3, 7 and 10 atmospheres, which correspond to conditions most often seen in PSA processes. As can be seen in Figure 15, carbon dioxide shows an adsorption capacity superior to that of nitrogen, even being in lower concentration in the flue gas. The pure amount adsorbed of both elements at 313 K is also plotted for comparison purposes.

The conclusion that we can extract from this figure is that, as expected, the amount adsorbed of carbon dioxide is higher than the nitrogen, although 68% lower from the obtained as pure gas. This fact increases while pressure increases, and is due to the difference of adsorbed molar fractions. While the amount of CO_2 increases with pressure, that of N_2 remains practically constant; this is because the CO_2 molecules occupy the available spaces for the separation without allowing more N_2 molecules.

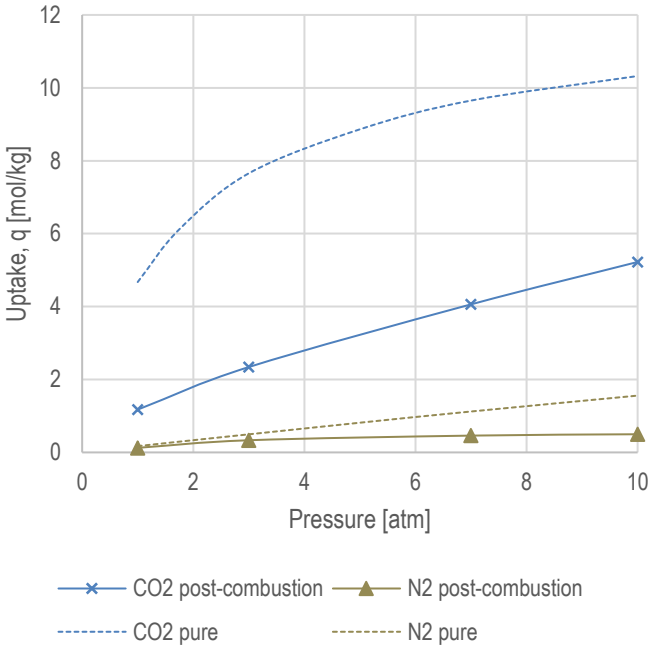

Figure 15. Comparison between CO_2 and N_2 adsorption from pure and mixture (15%CO_2/85%N_2) streams.

Taking into account the adsorption isotherms from Figure 14, it is known that the presence of SO_2 will decrease the amount of CO_2 and N_2 adsorbed. For the purpose of comparing the impurity effect in the total adsorption of CO_2, simulations for mixtures with 1% SO_2 (15% CO_2, 84% N_2) and 0.2% (15% CO_2, 84.8% N_2) have been carried out for pressures of 1 and 10 atmospheres and at a temperature of 313 K. In Figure 16, the adsorption [in mol/kg] of CO_2 for these mixtures is compared with the results without sulfur dioxide from the previous subsection.

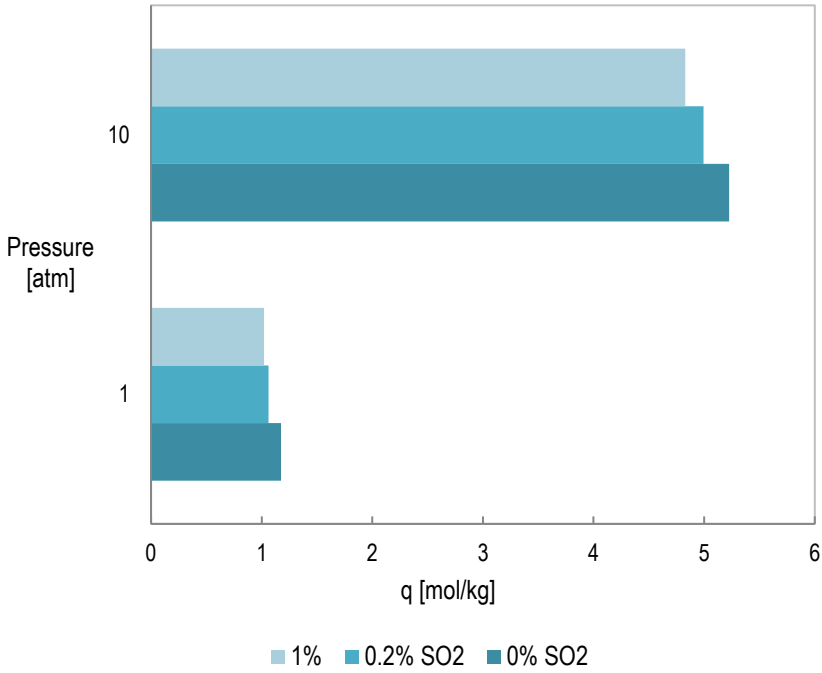

Figure 16. CO_2 adsorption uptake in post-combustion CO_2/N_2 separation with SO_2 impurities.

As already predicted, the plot shows a decrease in the CO_2 adsorption with the presence of SO_2. This decrease is due to the strong affinity of SO_2 with the adsorbent. At a pressure of 10 atmospheres it can be observed that the adsorption decreases almost 7.5% (5.22 to 4.83 mol/kg) with only 1% of SO_2, and at 1 atmosphere the decrease is about 4.4%. Although this impurity reduces the CO_2 adsorption, the MOF material continues to be a good adsorbent for this mixture, since the adsorption of this compound is still higher than that of nitrogen.

To verify this fact, the selectivity of carbon dioxide with respect to nitrogen for different pressures and concentrations of SO_2 is plotted in Figure 17.

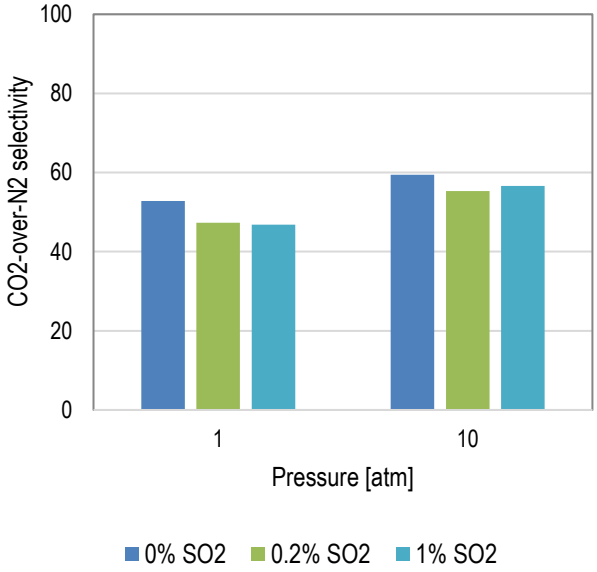

Figure 17. CO_2/N_2 selectivity in Ni-MOF-74 for post-combustion streams with SO_2 traces.

The selectivity depends on the composition of the feed stream, as well as the adsorbent-adsorbate interactions. To achieve a suitable separation, it is important that the selectivity of the component to be separated is as high as possible. As it was expected, SO_2 decreases CO_2 selectivity in almost 10%. Therefore, it would be important to perform a SO_2 removal process prior to adsorption (in case the fuel contains sulfur).

6.3.1.1. Regeneration by Swing Adsorption Processes

Once the adsorption is investigated, the desorption possibilities have to be analyzed. Therefore, different swing adsorption process will be compared in this section: TSA, PSA, VSA will be studied as well as combined ones such as VPSA.

A total of eight representative desorption conditions were evaluated for typical swing adsorption processes. Temperature swing adsorption has been evaluated considering a current feed at 313 K and providing heat to the system until reaching a temperature of 413 K (*i.e.*, 140°C,

a bit higher than to the values for absorption regeneration) at which desorption will occur. PSA and VSA will be achieved by exerting compression and decompression works, respectively. Pressure swing adsorption was evaluated with adsorption pressures of 3, 7 and 10 atmospheres, and a desorption step at atmospheric condition. In addition, VSA method consider an entrance at atmospheric pressure that was reduced at pressures from 0.05 to 0.15 atmospheres. In addition, three extra conditions were calculated for VPSA, named 10atm→0.05atm, 7atm→0.05atm and 3atm→0.05atm, representing compression at 10, 7 and 3 atm, and using vacuum up to 0.05 atm for desorption.

First of all, the working capacity for the different swing adsorption processes is presented in Figure 18. Being the working capacity a reference to the amount desorbed, it is convenient that it be the highest possible. Furthermore, the energy required to achieve this desorption has been also plotted with a grey line.

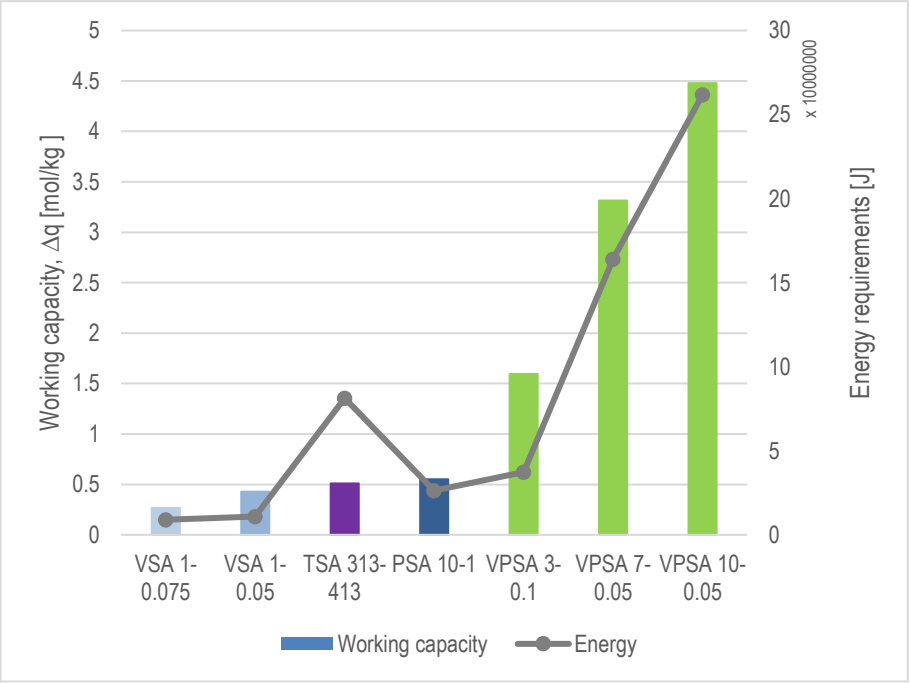

Figure 18. Working capacity for different Swing Adsorption processes.

It can be observed that higher working capacities are achieved with the VPSA method. In fact, this is expected since it is the method with the maximum pressure difference. However, as has already mentioned, it is important that the working capacity be as high as possible, but it does not determinate the best swing adsorption process. It is also important to minimize the energy used to carry it out. For this reason, Figure 18 also shows the energy requirements for each process, and it can be seen than the tendency is very similar for the one obtained with Δq.

The working capacity has been plotted in Figure 19, but in this case vs. the energy index (in units of Giga joules per tons of CO_2 desorbed) necessary to achieve this conditions. It is shown that the method that provides a higher Δq also needs a higher energy index. In addition, it can be observed that the PSA method requires a high energy index to achieve a low working capacity, so it can be concluded that this will not be an effective method for this type of mixture.

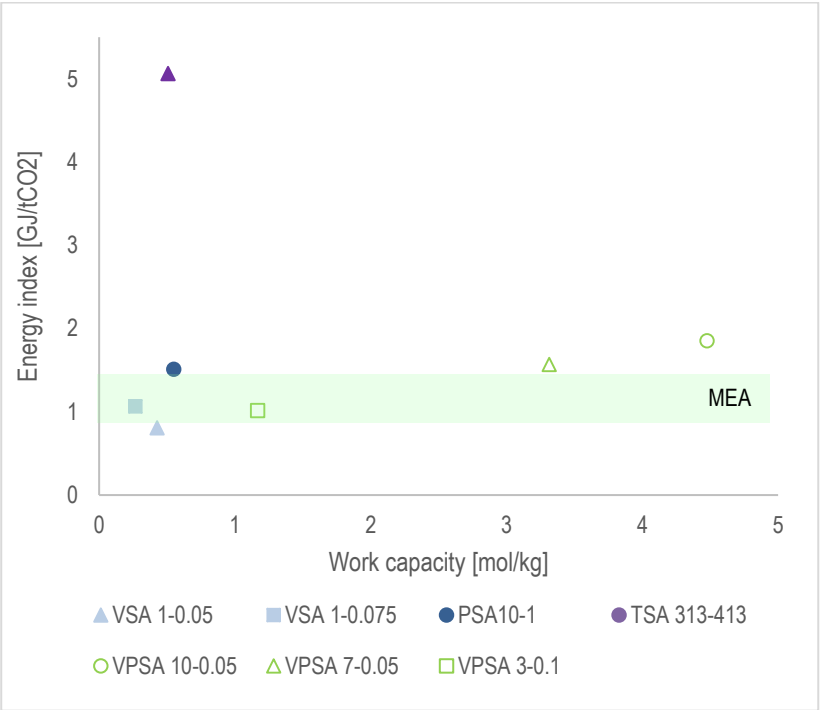

Figure 19. Working capacity VS Energy requirements for post-combustion gases

Since in Figure 19 it is difficult to compare and quantify the different methods of swing adsorption, and in addition, the energy required for the TSA method is not the same as the rest, it has been decided to calculate the energetic demand that this process represents of the total generated by a power plant. As already mentioned in the methodology (see Chapter 5), a typical scheme as the one shown in Appendix 2 was used to perform the calculations. The results are shown in Table 5, as well as the working capacity of the processes and the number of cycles to recover one tonne of CO_2 (assuming a $1m^3$ of bed with ε=0.4).

	Δq *[mol/kg]*	*Consumed Energy [%]*
VSA 1atm → 0.05atm	0.4	**14.6**
PSA 10atm → 1atm	0.6	**27.2**
VPSA 10atm → 0.05atm	4.5	**33.4**
VPSA 7atm → 0.05atm	3.3	**28.3**
VPSA 3atm → 0.1atm	1.2	**18.3**
TSA 313K → 413K	0.5	**59.2**

Table 5. Energy required of the generated in the power plant, for each post-combustion swing adsorption process

As it is observed, TSA method is the one which requires the highest energy percentage. In addition to that, VSA method is the best candidates, with lower values than PSA and VPSA. Although, VPSA of 3 atmospheres up to 0.1, presents similar values.

The conclusion obtained from the previous table is that this MOF have the potential to significantly decrease the energy ratio required for this process compared to a current technology with amines. The data obtained with the computational simulation is an approximation quite similar to reality, as has been demonstrated in the validation. For this reason, a technology with which 15% of consumption is expected is very likely to lead a significant reduction in the energy costs of the plant. In addition, it can be predicted that the adsorption method that, for this mixture, promises a lower energy requirement of the total plant, is the VSA with 1 atm and 0.05 atm as adsorption and desorption pressures.

With the aim of studying the effect of SO_2 on post-combustion streams and check if VSA method continues to be effective with the presence of this component, working capacities with

different concentrations of SO_2 (0.2% and 1%), as well as, without impurity, have been compared in Figure 20.

Hence, a decrease in working capacity by increasing the concentrations of SO_2 can be observed. Moreover, it can be detected that this magnitude is still higher for VPSA than for the rest of swing adsorptions. The energy requirements of the total plant are presented in Table 6.

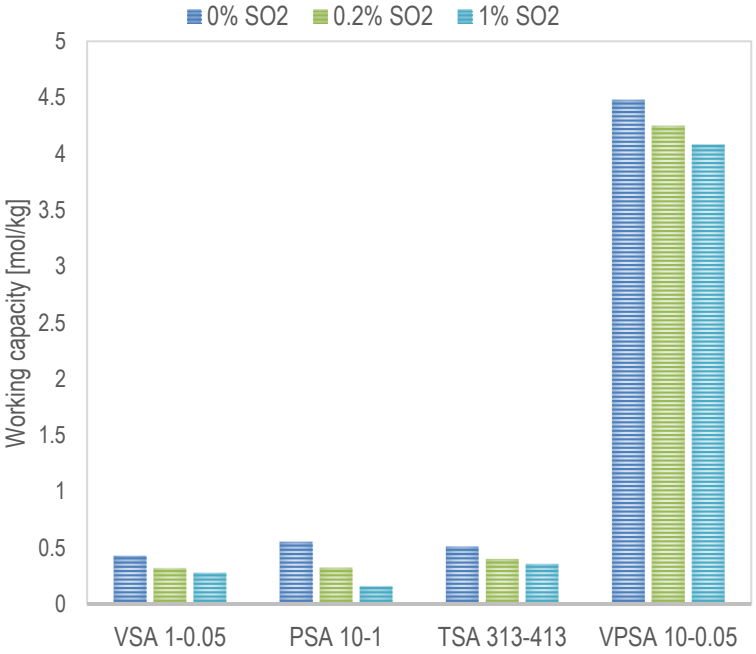

Figure 20. Effect of SO_2 on working capacity for post-combustion mixtures. 15% CO_2 in all ternary mixtures, while N_2 was taken as the surplus.

requirements [%] of the energy generated			
	0% SO_2	**0.2% SO_2**	**1% SO_2**
VSA 1 atm → 0.05 atm	14.6	19.7	27.3
PSA 10 atm → 1 atm	27.2	35.6	41.4
VPSA 10 atm → 0.05 atm	36.4	36.5	36.6
VPSA 10 atm → 0.075 atm	35.0	35.1	35.1
VPSA 10 atm → 0.1 atm	30.6	30.7	30.8
TSA 313 K → 413 K	59.2	73.6	81.3

Table 6. Energy requirements for post-combustion mixtures with SO_2 impurities.

As it could be predicted, the most suitable swing adsorption process continues to be VSA, the value of which has increased by 5% with the small amount of 0.2% SO_2. However, the VPSA method is almost unaffected by the presence of SO_2.

6.3.2. SYNGAS AND BIOGAS

In addition to post-combustion gases, mixtures of syngas (30% CO_2, 70% H_2) and biogas (50% CO_2 / 50% CH4, and 40% CO_2 / 60% CH4) have also been studied for the purpose of studying the adequate method of CO_2 adsorption for different gas streams in which this component is involved. Therefore, the CO_2/H_2 and CO_2/CH_4 separations have been calculated.

The results of these studies can be found in more detail in Appendix 4. A brief summary is presented below; first, working capacities for these mixture streams are shown in Figure 21 for the different swing adsorption method evaluated.

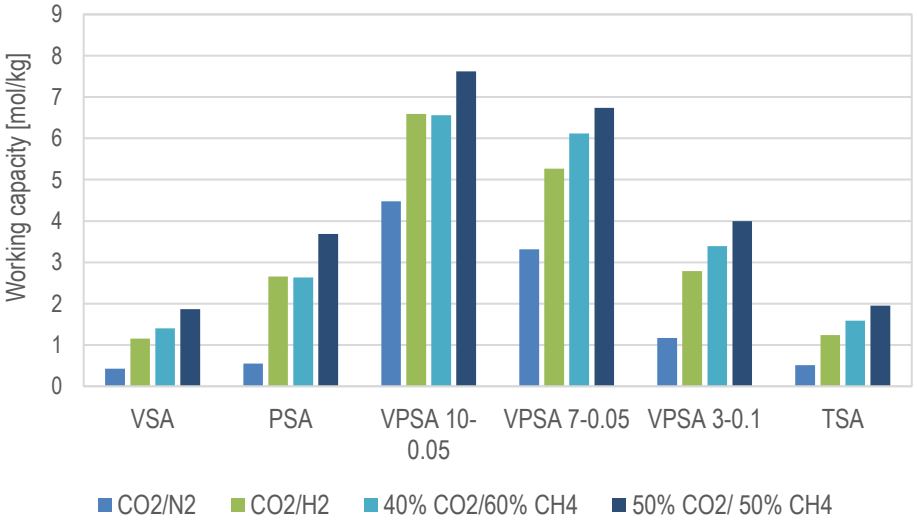

Figure 21. Working capacity for different mixture separations.

As already observed, VPSA cycles present higher working capacities but also higher energy requirements. In addition, it is shown that the separation presenting a higher working capacity is

the biogas 50%-50%. It is interesting that, although the adsorption is lower for pure hydrogen than methane, the earlier is present in higher amounts (70% hydrogen versus 50% methane). It can also be appreciated in biogas mixture that the higher CO_2 concentration, the higher working capacity will present.

In order to be able to compare all the swing adsorption processes evaluated, Table 7 presents the most suitable swing adsorption method and the energy requirements of each current through different sequences.

In the case of post-combustion, methane is supposed to be used as pure fuel, so there is only one possible sequence in which methane is burned producing CO_2 and being adsorbed subsequently (*comb-sep*). In the syngas mixture, the sequences are: *sep-comb* where the CO_2 is previously separated from hydrogen and then the latter is burned, and *comb-sep* where the fuel is burned in presence of carbon dioxide and then is separated. For biogas, fuel can be burned in the presence of CO_2 (which will lower the efficiency) (*comb-sep*) or carbon dioxide can be removed from methane and then separate the typical CO_2/N_2 post-combustion mixture (*sep-comb-sep*). Since this former mechanism depends on two separations, only the combination of the most effective separations was studied: VSA from 3 to 0.05 atmospheres in CO_2/CH_4 and VSA from 3 to 0.15 atmospheres in CO_2/N_2 separations (VSA-VSA)

Mixture	Sequence	Swing adsorption	% Energy
POST-COMBUSTION	comb-sep	VSA 1 atm→ 0.05 atm	14.6
SYNGAS	sep-comb	VSA 1 atm → 0.05 atm	12.3
	comb-sep	VPSA 3 atm → 0.1 atm	13.4
BIOGAS 40%CO_2-60%CH_4	sep-comb-sep	VSA → VSA	58.3
	comb-sep	VSA 3 atm → 0.05 atm	15.5
BIOGAS 50%CO_2-50%CH_4	sep-com-sep	VSA→VSA	43.7
	comb-sep	VSA 3 atm → 0.05 atm	15.8

Table 7. Most suitable swing adsorption processes found for each mixture type studied: Post-combustion, Syngas, and Biogas.

The results herein clearly show that there is no a unique swing adsorption condition for carbon capture, since it depends dramatically on the process. The lower energy percentage of the power supplied by the thermal plant was obtained for separating syngas. In fact, this was

expected as the difference of adsorption, shown in Figure 13, is higher for the mixture of carbon dioxide and hydrogen. However, in Figure 21 the methane separation presented higher working capacities. For this case, in syngas mixture the sequence is not too important, since they have similar energetic consumption.

It is expected that higher concentration of CO_2 in the fuel feed stream will increases the energy required for the separation. Therefore, biogas with 40% CO_2 and 60% of CH_4 will have a better performance than the 50%-50% mixture. Although the adsorption of methane is higher than that of nitrogen, it is convenient to carry out the combustion in presence of CO_2 inasmuch as the execution of two separations significantly increases the energy requirements.

7. CONCLUSIONS

- As it has been proved in the validation, simulation results follow the trend of those obtained experimentally, approaching them significantly. Therefore, it could be said that the parameters used in the simulation as well as the method are correct.
- Carbon dioxide presents a significantly higher adsorption capacity that the components present in the mixtures studied, such as CH_4, H_2, and N_2. Thereupon, Ni-MOF-74 promises to be a suitable adsorbent to separate CO_2 from these currents.
- However, sulphur dioxide can represent an issue in the CO_2 adsorption as its adsorption in higher than that of carbon dioxide. This fact will cause the rapid adsorption of SO_2 occupying the pores of the MOF that will not be able to adsorb the desired component.
- For post-combustion gases, VSA method was found to be the most effective for capturing CO_2 in post-combustion streams. The lower energy requirements for this mixture, are obtained with a feed stream at ambient pressure to which the vacuum is made up to 0.05 atmospheres to carry out the desorption. In that way, CO_2 adsorption by Ni-MOF-74 in a post-combustion mix could represent only a 14.6% consumption of the total electric energy produced by the fuel, even lower than the technology with amine solvents. So that, the technology studied promises a significant reduction in CO_2 capture for post-combustion gases.
- Moreover, the presence of impurities, such as SO_2, increases the energy requirements between 5-13% with an amount of 0.2 and 1% of Sulphur dioxide respectively.
- In the case of biogas, it is preferable to carry out a combustion with the presence of CO_2 and then perform a CO_2/N_2 separation with VSA method. This sequence requires a total of 15.8% in the case of the mixing equal parts of methane and

carbon dioxide, and 15.5% for the mixture by 40% CO_2 and 60% CH_4 of the energy generated.

- For syngas, a 12.3% of the total electric energy generated should be required for carbon dioxide capture. For this separation, a simple VSA (decreasing pressure until 0.05 atm) is the preferred method to use before or after combustion.
- The Thermal Swing Adsorption (TSA) method presents the higher energy requirements for all the mixtures, which makes it an unfeasible method.
- The calculations made for this project have been obtained with equilibrium thermodynamic parameters. To determinate if the VPSA is the most suitable method, it would be necessary to carry out a more detailed study in which the kinetic parameters are required, as well as, the simulation of the whole process.

8. REFERENCES AND NOTES

1. Arunkuman, S.; Zhao, A.; Shimizu, G. K. H.; Sarkar, P.; Gupta, R. Post-Combustion CO_2 Capture Using Solid Sorbents: A Review, *Ind. Eng. Chem. Res*.**, 2012,***51*, 1438.
2. Li, J. R.; Ma, Y.; McCarthy, M. C.; Sculley J.; Yu, J.; Jeong, H. K.; Balbuena, P. B.; Zhou, H. Carbon dioxide capture-related gas adsorption and separation in metal-organic frameworks. *Coordination Chemistry Reviews*, **2011,** *255*(15), 1791-1823.
3. Wang, Y.; Zhao, L.; Otto, A.; Robinius, M.; Stolfen, D. A Review of Post-combustion CO_2 Capture Technologies from Coal-fired Power Plants. *Energy Procedia*, **2017**, 114, 650-665.
4. Dickey, A. N.; Özgür, A.; Willis, R. R.; Snurr, R. Q.; Screening CO_2/N_2 selectivity in Metal-Organic Frameworks using Monte Carlo simulation and ideal adsorbed solution theory. *The Canadian Journal of Chemical Engineering*, **2012,** *90*(4), 825-832.
5. Wells, B. A.; Webley, P. A.; Chaffee, A. L. Simulations of model metal-organic frameworks for the separation of carbon dioxide. *Energy Procedia* **2011**, 4, 568-575.
6. Hu, J.; Ma, A.; Dinner, A. R. Monte Carlo simulations of biomolecules: The MC module in CHARMM. *J Comp.Chem*. **2006,** *27*, 203-216.
7. Mercado, R.; Vlaisavljevich, B.; Lin, L.; Lee, K.; Lee, Y.; Manson, J. A.; Gonzalez, M. I; Kapelewski, M.; Neaton, J.; Smit, B. Force Field Development from Periodic Density Functional Theory Calculations for Gas Separation Applications Using Metal-Organic Frameworks. *The Journal of Physical Chemistry C*, **2016,** *120*(23), 12590-12604.
8. Sabouni, R.; Kazemian, H.; Rohani, S. Carbon dioxide capturing technologies: a review focusing on metal oganic framework materials (MOFs), *Environmental Science and Pollution Research,* **2014,** *21* (8), 5427–5449.
9. He, X.; Hägg, M.B. Membranes for Enviromentally Friendly Energy Processes. *Membranes*, **2012,** *2*, 706-726.
10. Simmons, J. M.; Wu, H.; Zhou, W.; Yildirim, T. Carbon capture in metal-organic frameworks - A comparative study. *Energy & Enviromental Science*, **2011,** *4*, 2177.
11. IUPAC. International Union of pure and applied chemistry. https://iupac.org (accessed May 5, 2018).
12. Sarabadan, S. Adsorptive air separation behavior on silver exchanged ETS-10 Typed Molecular Sieves, **2011.** PhD Thesis.
13. Tagliabue, M.; Farrusseng, D.; Valencia, S.; Aguado, S.; Ravon, U.; Rizzo, C.; Corma, A.; Mirodatos, C. Natural gas treating by selective adsorption: Material science and chemical engineering interplay. *Chemical Engineering Journal*, **2009,** *155*(3), 533-566.
14. Alothman, Z. A Review: Fundamental Aspects of Silicate Mesoporous Materials, *Materials* **2012,** *5*(12), 2874-2902.
15. Thommes, M.; Kaneko, K.; Neimark, A. V.; Olivier, J. P.; Rodriguez-Reinoso, F.; Rouquerol, J.; Sing, K. S. W. Physisorption of gases, with special reference to the evaluation of surface area and pore size distribution (IUPAC Technical Report), **2015.**

16. Zhao, Y.; Song, Z.; Li, X.; Sun, Q.; Cheng, N.; Lawes, S.; Sun, X. Metal organic frameworks for energy storage and conversion. Energy Storage Materials, **2016,** *2*, 35-62.
17. Albuquerque, G. H.; Fitzmorris, R. C.; Ahmadi, M.; Wannenmacher, N.; Thallapally, P. K.; McGrail, B. P.; Herman, G. S. Gas-Liquid segmented flow microwave-assisted synthesis of MOF-74(Ni) under moderated pressures. *CrystEngComm*, **2015**,*17*, 5502-5510**.**
18. Shi, B.; Al-Dadah, R.; Mahmoud, S.; Elsayed, A.; Elsayed, E. CPO-27 (Ni) Metal-Organic Framework Based Adsorption System for Auto-motive Air Conditioning. *Applied Thermal Engineering*, **2016,** *106*-325-333.
19. Wang, H.; Qu, Z. G.; Zhang, W.; Chang, Y. X.; He, Y. L. Experimental and numerical of CO_2 adsorption Ni/DOBDC metal-organic framework. *Applied Thermal Engineering*, **2014,** *73*(2), 1501-1509.
20. Liu, J.; Wang, Y.; Benin, A. I.; Jakubczak, P.; Willis, R. R.; LeVan, M. D. CO_2/H_2O Adsorption Equilibrium and Rates on Metal-Organic Frameworks: HKUST-1 and Ni/DOBDC. *Langmuir*, **2010**, *26* (17), 14301–14307**.**
21. Hedin, N.; Andersson, L.; Bersgtröm, L.; Yan, J.; Adsorbent for the post-combustion capture of CO_2 using rapid temperature swing or vacuum swing adsorption. *Applied Energy,* **2013,** *104*, 418-433.
22. Simmons, J. M.; Wu, H.; Zhou, W.; Yildirim, T. Carbon capture in metal-organic frameworks- a comparative study. *Energy & Enviromental Science*, **2011,** *4*, 2177.
23. GSTC: Syngas production. https://www.globalsyngas.org (accessed May 20, 2018).
24. Ecobiogas. http://www.ecobiogas.es (accessed May 20, 2018).
25. Global CCS Institute: CO_2 reuse technologies. https://hub.globalccsinstitute.com/publications/accelerating-uptake-ccs-industrial-use-captured-carbon-dioxide/1-co2-reuse-technologies (accessed May 19, 2018).
26. Erucar, I.; Keskin, S. High CO_2 Selectivity of an Amine-Functionalized Metal Organic Framework in Adsorption-based and Membrane-based Gas Separations. *Ind. Eng. Chem. Res., **2013**, 52 (9), 3462–3472.*
27. Torrens, I.M. Interatomic potentials. Academic Press, New York. **1972.**
28. Gutiérrez, G. Elementos de simulación computacional, **2001.**
29. Frenkel, D.; Smit, B.; Understanding Molecular Simulations from algorithms to applications. Academic Press, San Diego. **2002,** 2nd ed.
30. González, J.; Demontis, P.; Baldovino, G.; Métodos deterministas y estocásticos aplicados al estudio de materiales microporosos. *Revista CENIC Ciencias Químicas,* **2010**, *41*, 85-98.
31. Becker, T. M.; Heinen, J.; Dubbeldam, D.; Lin, L.; Vlught, T. J. H. Polarizable Force Fields for CO_2 and CH_4 Adsorption in M-MOF-74. *J. Phys. Chem. C*, **2017**, *121*,4659.
32. Potoff, J.J.; Siepmann, J. I. Vapor–liquid equilibria of mixtures containing alkanes, carbon dioxide, and nitrogen, *AIChE J*.**, 2001,** *47, 1676–1682.*
33. Ketko, M. H.; Kamath, G.; Potoff, J. J. Development of an optimized intermolecular potential for sulfur dioxide, *J. Phys. Chem. C,* **2011,** *115* (17), 4949–4954.
34. Queen, W. L.; Hudson, M. R.; Bloch, E. D.; Mason, J. A.; Gonzalez, M. I.; Lee, J. S.; Gygi, D.; Howe, J. D.; Lee, K.; Darwish, T. A.; et al. Comprehensive Study of Carbon Dioxide Adsorption in the Metal–organic Frameworks M_2(DOBDC) (M = Mg, Mn, Fe, Co, Ni, Cu, Zn). *Chem. Sci*. **2014,** *5*(12), 4569–4581.

ACRONYMS

AC	Activated Carbon
Cp	Heat Capacity [J/mol K]
LJ	Lennard-Jones
MC	Montecarlo
MD	Molecular Dynamic
MOFs	Metal Organic Frameworks
N	Number of species
$\mathcal{N}$	Number of molecules adsorbed at each condition in MC simulations
k	Polytropic parameter of gases
K	Henry's constants
P	Pressure [atm]
PSA	Pressure Swing Adsorption
r_{ij}	Distance between two atoms, *i* and *j*
Q	Charges of the atoms
q_{ads}	Amount adsorbed [mol/kg]
q_{des}	Amount desorbed [mol/kg]
q_{st}	Isosteric heat of adsorption [kJ/mol]
R	Gas constant [8.314 kPa m^3/ kmol K]
T	Temperature [K]
TSA	Temperature Swing Adsorption
$U_{i/j}$	Potencial energy between a pair of atoms *i* and *j* [kJ/mol]
U	Total potencial energy of a system, or of an isolated guest molecule [kJ/mol]

VSA	Vacuum Swing Adsorption
x	Mole fraction of a component in the adsorbed phase
y	Mole fraction of a component in the gas phase
$\alpha_{i/j}$	Selectivity from *i* vs *j*
Δq	Working capacity [mol/kg]
ϵ	Voidage of bed
ϵ_{LJ}	Lennard-Jones potencial [kJ/mol]
η	Feeding/vacuum blower efficiency
σ_{ij}	Lennard-Jones potencial diameter [Å]
ρ	Framework density [kg/m ^{3}]

INDEX OF FIGURES AND TABLES

Figures

Tables

APPENDICES

APPENDIX 1: SIMULATION STABILITY

The following figure shows the 1,000,000 steps of Monte Carlo for one simulation (*e.g.,* pure CO_2 at 313K and at a pressure of 1atm). The first 500,000 steps have been considered necessary to guarantee that the system has reached equilibrium (shown in orange in Figure A1) and the rest of steps have been taken as production data and have been used to obtain the final average value (in blue). Each one of these plots represents a point of the isotherms.

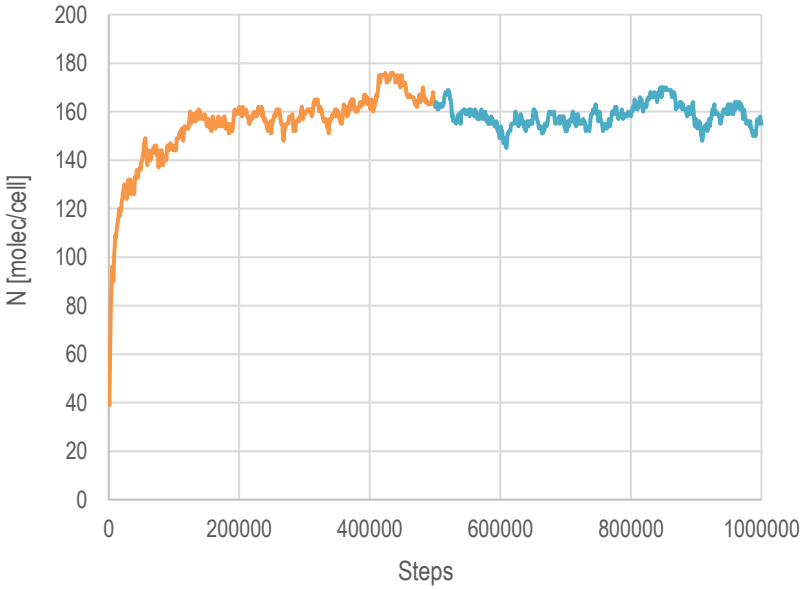

Figure A1. Simulation stability: Number of molecules adsorbed vs. MC steps

AVERAGE [molec/cell]	σ^2 [mol/cell]
158.44	4.74

Table A1. Simulation average

APPENDIX 2: ELECTRIC POWER PRODUCTION DIAGRAM

In this section, an example diagram is presented with respect to the scheme used for the energy requirements calculations. In this case, it would be the one used for PSA system of post-combustion mixture.

The electricity generation system consists of a unit where combustion takes place. The hot gases are used to raise the temperature of a stream, which generates electricity in the turbine by means of a cycle.

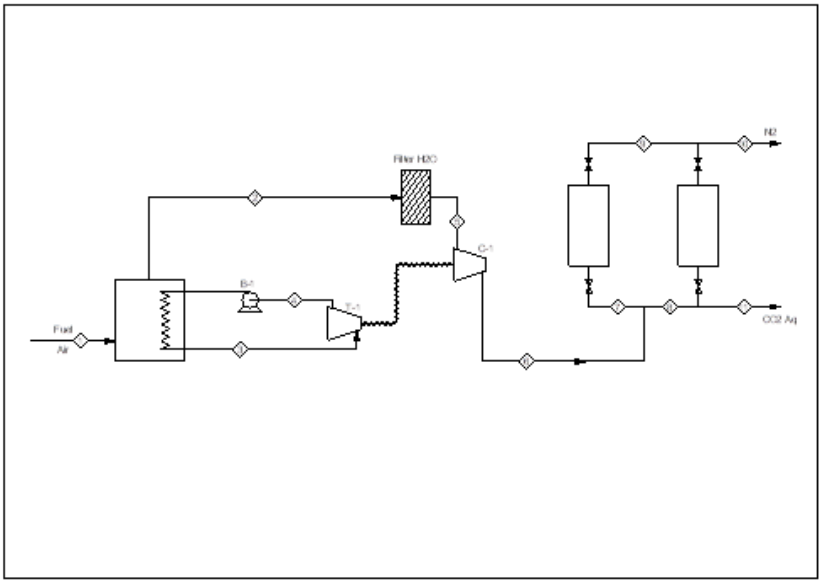

Figure A2. Electric power production scheme

Combustion gases are afterwards cooled to water condensation, where the latter is filtered and the mixture (CO_2/N_2) is taken to a CO_2 separation and capture system. This equipment consists of two columns to resemble a continuous process.

As can be seen, part of the electricity generated is used to drive a compressor that raises the pressure of the inlet gas to the adsorbers.

Finally, there are two practically pure product streams: N_2, which passes through the beds without being adsorbed, and the CO_2 recovered after the depressurization stage.

APPENDIX 3: ISOTHERM PARAMETRIZATION

Adsorption isotherms of pure components can be parametrized using Langmuir of Freundlich models with the following equations:

- **LANGMUIR:** $q = \frac{q_{sat} \cdot b \cdot P}{1 + b \cdot P}$
- **FREUNDLICH:** $q = m \cdot P^{1/n}$

The component with higher adsorption (CO_2, SO_2) adjust better to Langmuir method while those with less adsorption to the Freundlich one at the pressure range studied. It should also be noted that the correlations are close to one.

LANGMUIR			
Component	**q_{sat} [mol/kg]**	**B [1/atm]**	**R^2**
CO_2	11.66	0.94	0.9976
SO_2	11.06	13.49	0.9998
FREUNDLICH			
Component	**M [mol/kg.atm]**	**n**	**R^2**
N_2	1.54	0.92	0.979
CH_4	0.32	0.9	0.9945
H_2	0.03	0.96	0.9908

Table A2. Langmuir and Freundlich parameters obtained for each molecule adsorbed on Ni-MOF-74.

APPENDIX 4: OTHER MIXTURES

- **CO_2/H_2 separation. Syngas**

The working capacities of a syngas mixture of CO_2 and H_2 is presented in Figure A3.

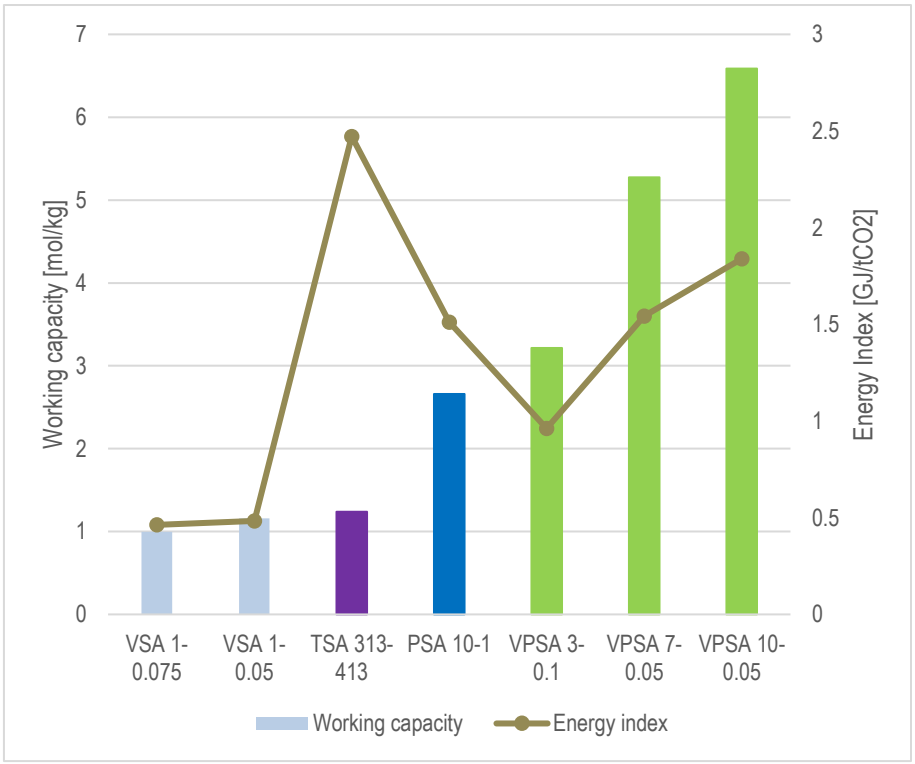

Figure A3. Working capacities and energy index for swing adsorption processes on syngas mixtures (70% H_2 / 30% CO_2).

As it was expected, the higher working capacity is achieved with the VPSA method, although to consider this method as the most efficient it is necessary to make an energy comparison. These results are presented in Table A3.

		VSA	PSA	VPSA 10-0.05	VPSA 7-0.05	VPSA 3-0.1	TSA
SYNGAS	sep-comb	**12.3**	38.4	46.7	39.2	22.7	79.23
	comb-sep	**13.8**	28.9	31.7	16.0	**13.4**	57.9

Table A3. Energy requirements [%] for syngas

In this case, two different sequences have been used: combustion in presence of carbon dioxide and subsequent separation (*comb-sep*) and capture of CO_2 prior to combustion. It can be observed that for both mechanisms, the most effective method is the VSA in which the vacuum is made up to a pressure of 0.05 atmosphere, as well as, the VPSA method of 3 to 0.1 atmospheres can be incorporated in the combustion-separation sequence, with similar energy requirements. In addition, the difference in energy requirement between them is insignificant, which could be considered that both sequences would be effective.

- **CO_2/CH_4 separation. Biogas**

This section shows the results of carbon dioxide capture and separation from 50%CO_2 / 50%CH_4 and 40%CO_2 / 60%CH_4 mixture streams (see Figures A4 and A5)

Figures A4 and A5 show the dependence of working capacity and energy requirements with the composition of the current feed. It is observed that higher amount of CO_2 in the mixture presents a greater working capacity. In fact, this is expected since there is more affine compound to adsorb. It is already known that a higher working capacity does not imply a better adsorption method. Table A3 shows which technique requires less energy.

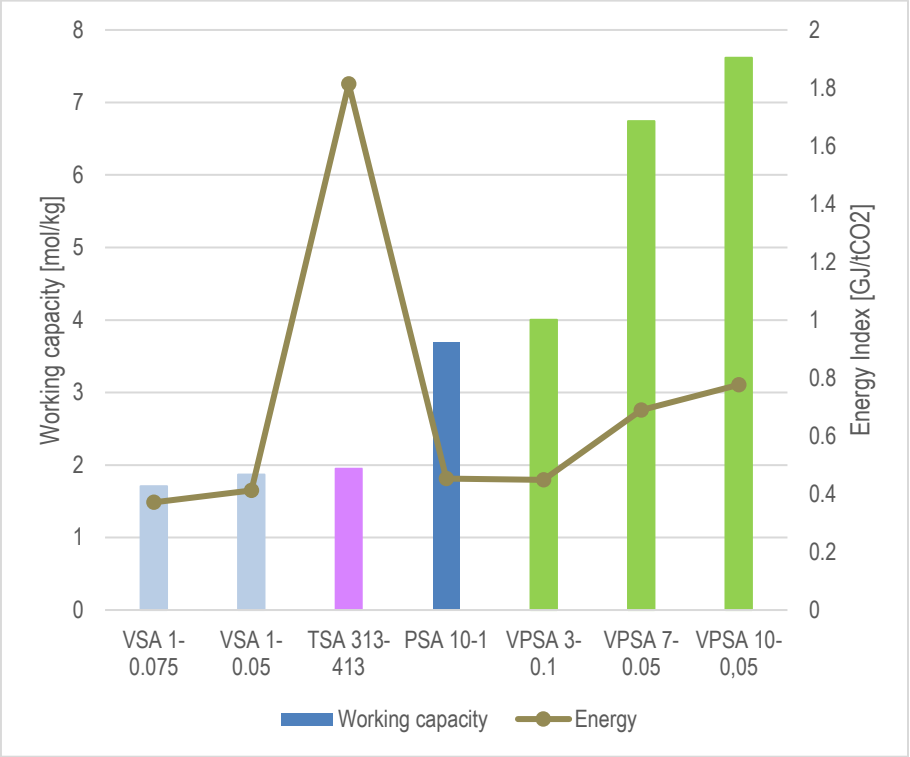

Figure A4. Working capacities and energy index for swing adsorption processes for biogas mixture of 50% CO_2 and 50% CH_4.

For both compositions, two different sequences have been proposed: combustion with CO_2 present and subsequent CO_2/N_2 separation (in Table A3) and separation of the fuel and subsequent capture of CO_2 formed by combustion (in Table A4). Both sequences are shown below. Noted that the data obtained through the separation-combustion-separation sequence is presented only for the combination of the two optimal methods studied: VSA 1atm→0.05atm for CO_2/N_2 separation and VSA 1atm→0.15atm for CO_2/CH_4.

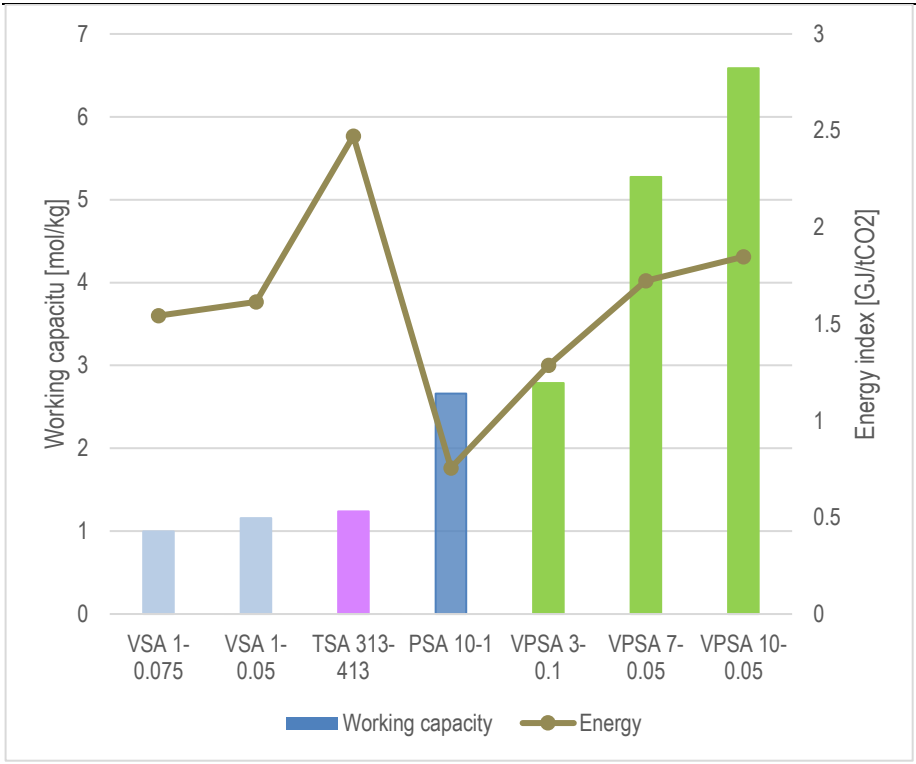

Figure A5. Working capacities and energy index for swing adsorption processes for biogas mixture of 40% CO_2 and 60% CH_4.

	VSA	PSA	VPSA 10-0.05	VPSA 7-0.05	VPSA 3-0.1	TSA
BIOGAS 50-50	**15.8**	29.5	31.3	27.8	21.7	111
BIOGAS 40-60	**15.5**	29.0	30.8	27.3	21.4	98.7

Table A3. Energy requirements for biogas combustion-separation

	VPSA-VPSA
BIOGAS 50-50	**58.3**
BIOGAS 40-60	**43.7**

Table A4. Energy requirements for biogas in separation-combustion-separation

The most efficient sequence for biogas is the combustion in presence of CO_2 and subsequently a CO_2/N_2 separation. From this separation it can be noted that, as in the previous mixtures, the TSA method presents the higher energy requirements, in this case higher or equal to the energy delivered.